8-2016

The Immune Microenvironment of Microsatellite Instable Endometrial Cancer

Janelle B. Pakish

The Immune Microenvironment of Microsatellite Instable Endometrial Cancer

by

Janelle Beth Pakish, M.D.

APPROVED:

Karen Lu, M.D
Advisory Professor

Melinda Yates, Ph.D.

Samuel Mok, Ph.D.

Russell Broaddus, M.D., Ph.D.

Padmanee Sharma, M.D., Ph.D.

APPROVED:

Dean, The University of Texas

Graduate School of Biomedical Sciences at Houston

The Immune Microenvironment of Microsatellite Instable Endometrial Cancer

A

THESIS

Presented to the Faculty of the

The University of Texas

Health Science Center at Houston

and

The University of Texas

MD Anderson Cancer Center

Graduate School of Biomedical Sciences

in Partial Fulfillment

of the Requirements

for the Degree of

MASTER OF SCIENCE

by

Janelle Beth Pakish, M.D.

Houston, Texas

August, 2016

Acknowledgements

I would first like to thank my thesis mentor, Dr. Karen Lu. Her mentorship and guidance during my research years have made it an extremely rewarding experience, and helped me to take my research to the next level. Thank you also to Melinda Yates for her close mentorship and continual support throughout my research. Her input and feedback was fundamental to the success of this work.

A special thank you to all the members of the Lu Lab for all the support, help, teaching, and friendship they provided. Thank you to Rosie Schmandt and Qian Zhang for showing me the ropes in the lab, and for their patience in teaching me various lab techniques. Thank you also to Joseph Celestino for all his behind the scenes help in moving this project forward.

Lastly, I'd like to thank my committee for all their thoughtful feedback and insight as this project has progressed over the last two years.

This work was supported in part by a NIH T32 grant, Training of Academic Gynecologic Oncologist, from the National Cancer Institute (5T32-CA101642).

The Immune Microenvironment of Microsatellite Instable Endometrial Cancer

Janelle Beth Pakish, M.D., M.S.

Advisory Professor: Karen Lu, M.D.

Limited treatment options are available for patients with advanced and recurrent endometrial cancer (EC) should standard chemotherapy fail. Recent studies in other tumor types have shown that tumors with high microsatellite instability (MSI-H) have increased immunogenicity and response to immunotherapy treatments compared to microsatellite stable (MSS) tumors. Patients with MSI-H EC may also benefit from these therapies; however, the tumor immune microenvironment in MSI-H EC has not yet been well described.

In order to evaluate the immune microenvironment of MSI-H EC, multiple approaches were used, including analysis of large publically available datasets and detailed characterization of patient tumor samples. Uterine cancer data from The Cancer Genome Atlas (TCGA) was used to study immune-related gene expression in MSI-H EC compared to MSS EC at both the individual gene and pathway level. Fluorescent multiplexing immunohistochemistry (IHC) was used to evaluate differences in immune cell populations using tumor specimens from these two groups followed by automated multispectral imaging and analysis to visualize and quantify staining in the tumor epithelial and stromal compartments. Nonparametric Mann-Whitney test was used to determine statistical significance (p value <0.05) of positive cell counts for CD3, CD4, CD8, CD103, CD68, CD11c, granzyme B, and PD-L1 between the groups.

Overall, MSI-H EC demonstrated increased immune activation compared to MSS EC. Using TCGA data, MSI-H (n=118) EC showed overall activation of the granzyme B signaling pathway compared to MSS (n=160) EC ($p < 0.01$). IHC analysis demonstrated increased granzyme B^+ cells (114.9 cells/mm^2 vs 75.8 cells/mm^2; $p<0.01$), activated cytotoxic T cells (CTLs) (45.6 cells/mm^2 vs 28.0 cells/mm^2; $p<0.01$), and PD-$L1^+$ cells (291.6 cells/mm^2 vs 240.5 cells/mm^2; $p<0.01$) in the stroma of MSI-H versus MSS ECs. The number of granzyme B^+ and activated cytotoxic T cells was also increased in the tumor epithelial compartment of MSI-H compared to MSS ECs. There was no difference in the other markers evaluated.

In conclusion, the immune microenvironment differs in MSI-H ECs with increased tumor immunogenicity compared to MSS tumors. Elevated PD-L1 expression also suggests immune response inhibition in these tumors, and patients with this subset of tumors are likely candidates for immune checkpoint blocking agents.

TABLE OF CONTENTS

List of Tables

List of Figures

List of Abbreviations

EC	endometrial cancer
OS	overall survival
LS	Lynch syndrome
MMR	mismatch repair
MLH1	human mutL homolog 1
MSH2	human mutS homolog 2
MSH6	human mutS homolog 6
PMS2	human postmeitotic segration 2
EPCAM	epithelial cell adhesion molecule
TCGA	The Cancer Genome Atlas
POLE	polymerase ε
MSI	microsatellite instability
CTNNB1	beta-catenin
MYH1	myosin 1
KRAS	Kirsten rat sarcoma viral oncogene homolog
IK	cytokine IK
MSI-H	high microsatellite instability
MSS	microsatellite stable
RR	response rates
PTEN	phospatase and tensin homolog
PI3K	phosphatidylinositiol 3-kinase

mTOR	mammalian target of rapamycin
CTL	cytotoxic T cell
TILs	tumor infiltrating lymphocytes
MHC	major histocompability
TCR	T cell receptor
NK	natural killer
TAM	tumor associated macrophage
CTLA-4	cytotoxic T lymphocyte associated protein 4
PD-1	programmed death 1
PD-L1	programmed death ligand 1
CRPC	castration-resistant prostate cancer
NSCLC	non-small cell lung cancer
CRC	colorectal cancer
HGSOC	high grade serous ovarian cancer
LAG-3	lymphocyte-activation gene 3
IDO	Indoleamine 2,3-dioxygenase
LS MSI-H	Lynch syndrome MSI-H
IHC	immunohistochemistry
RNAseq	RNA sequencing
SAM	significance analysis of microarrays
IPA	Ingenuity Pathway Analysis
TSA	tyramide signal amplification
DAPI	4',6-diamidino-2-phenylindole

HRP	horseradish peroxidase
IRB	Institutional Review Board
BMI	body mass index
FFPE	formalin fixed paraffin-embedded
MDACC	MD Anderson Cancer Center
PCR	polymerase chain reaction
AR	antigen retrieval
Cy3	cyanine 3
FITC	fluorescein
Cy5.5	cyanine 5.5
Cy3.5	cyanine 3.5
Cy5	cyanine 5
nm	nanometers
dH2O	distilled water
TBST	Tris-Buffered Saline with 0.05% Tween 20
μL	microliters
DMSO	dimethyl sulfoxide
mm^2	millimeters squared
LVSI	lymphovascular space invasion
kg/m^2	kilogram per meter squared
TIM-3	T cell immunoglobulin and mucin-domain containing-3

Chapter 1: Introduction

OVERVIEW

As the most frequent gynecologic malignancy in the Unites States, endometrial cancer (EC) is predicted to affect approximately 60,000 women in 2016 with a subsequent 10,500 EC related deaths (1). Due to the presence of early warning symptoms, such as postmenopausal bleeding, the majority of women with EC are diagnosed at an early stage (70%). Disease is typically localized to the uterus and has an associated 5-year overall survival (OS) of nearly 95% (2). In fact, most women with early stage disease are cured with hysterectomy alone (2). While the initial prognosis is positive, a subset of these patients will recur. Additionally, those women who have recurrent disease, or who are found to have advanced stage, have a worse prognosis with 5-year OS ranging from only 20-66% (3). Given the poor outcomes for recurrent and advanced disease, it is critical to identify key molecular subtypes amenable to targeted therapeutic strategies and to identify sub-groups that are more likely to recur.

Many factors are known to increase the risk of EC. Primarily, these risk factors include those that increase estrogen exposure like estrogen only hormone replacement therapy, obesity, early menarche, and late menopause. Inherited genetic syndromes, such as Lynch syndrome (LS), can also lead to increased risk of endometrial cancer. LS is an autosomal dominantly inherited disorder of a germline mutation in a DNA mismatch repair (MMR) gene that cause DNA MMR deficiency. These DNA MMR deficiency genes include: *MLH1* (human mutL homolog 1), *MSH2* (human mutS homolog 2), *MSH6* (human mutS homolog 6), *PMS2* (human postmeitotic segregation 2), and *EPCAM* (epithelial cell

adhesion molecule). Secondary to MMR deficiency, LS is associated with an elevated risk of developing EC, as well as, colorectal, ovarian, stomach, renal, ureteral, biliary tract, and central nervous system cancers (4). The lifetime risk of EC in women with LS is 60%, and about half will present with EC or ovarian cancer as their initial cancer diagnosis (4, 5). The specific risk of EC with *MSH6* mutations is 73%, 31% with *MLH1*, and 29% with *MSH2* (6), and more than 80% of LS-related ECs demonstrate endometrioid histology (4).

Overall, EC includes a wide spectrum of clinical, pathological, and molecular features that have been used to classify EC into different subtypes. Traditionally this included subdivision of EC into two categories (7). Type 1 tumors are the most common and consist mostly of the early stage and good prognosis cases described earlier. These tumors are also typically estrogen-dependent, of endometrioid histology, and low grade. Type 2 tumors, on the other hand, tend to be more aggressive, are of non-endometrioid histology, and have an overall worse prognosis. The Cancer Genome Atlas (TCGA) for uterine cancer created an integrated genomic characterization to provide a more sophisticated view of EC subtypes. The initial analysis of uterine cancer TCGA data included all tumors (multiple histologic subtypes together) and identified four unique groups characterized by somatic nucleotide substitutions (8). These groups included an ultramutated group of polymerase ε (POLE) mutations, a hypermutated group containing tumors with microsatellite instability (MSI), a low mutational rate group (copy-number low), and a copy-number high group comprising mostly non-endometrioid histology tumors. Later studies were conducted to characterize the molecular mechanisms underlying the observed clinical heterogeneity and identify subtypes at higher risk of recurrence. Liu et al. utilized the TCGA uterine data along with a separate validation tumor sample set to

perform molecular subtyping of endometrioid EC (9). In this analysis, they found four discreet subtypes of endometrioid EC that were defined by clinical, pathological, and mutational patterns. Cluster I consisted of tumors with low grade and stage along with increased expression of estrogen and progesterone receptors. Cluster II also contained low grade and stage tumors, but demonstrated worse survival and significantly more beta-catenin (*CTNNB1)* mutations. Cluster III and IV on the other hand, contained more advanced stage and advanced grade tumors, as well as, more P53 mutations. Myosin 1 (*MYH1)* and Kirsten rat sarcoma viral oncogene homolog (*KRAS)* mutations were also more frequently seen in Cluster III, and cytokine IK (*IK)* mutations were limited to Cluster IV. MSI was seen in all clusters, but represented half of cases in both Cluster III and IV and Lynch-related cases were not specifically examined. The different mutational profiles of these four clusters are demonstrated in Figure 1. Although our understanding of EC biology has advanced with these molecular classifications, these molecular fingerprints have not yet been translated to success using current targeted agents.

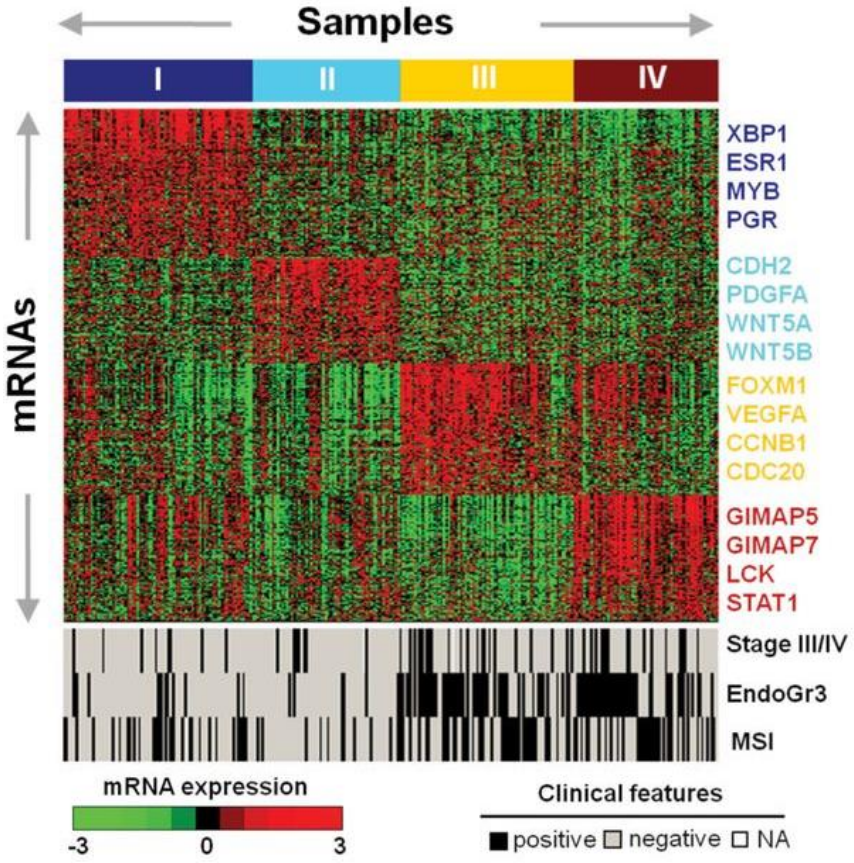

Figure 1. TCGA uterine cancer clusters by gene expression.

Distinct gene expression profiles are seen among the four endometrioid endometrial cancer subtypes. Red signifies normalized mRNA expression levels greater than the mean and green indicates those below the mean. Reproduced with permission from Oxford University Press: Liu Y, Patel L, Mills GB, Lu KH, Sood AK, Ding L, Kucherlapati r, Mardis ER, Levine DA, Shmulevich I, Broaddus RR, Zhang W, Clinical Significance of CTNNB1 Mutation and WnT Pathway Activation in Endometrioid Endometrial Carcinoma. J Natl Cancer Inst, 2014;106 (9).

LYNCH SYNDROME AND MICROSATELLITE INSTABILITY

One molecular subset of EC that has recently gained attention as a potential target for specific therapeutics is defined by microsatellite instability. This group includes both inherited LS-related and sporadic MSI EC, which both result from defects in DNA MMR. Damage to this pathway results in deficient repair of base pair mismatches that occur

during DNA replication (4). This deficiency then leads to multiple errors in areas of repetitive DNA sequences, known as microsatellites, resulting in microsatellite instability in these tumors (4). In sporadic MSI tumors, sporadic hypermethylation of the MLH1 promoter results in MMR deficiency and high microsatellite instability (MSI-H), and these are sometimes referred to as Lynch-like tumors. This hypermethylation specifically inactivates the *MLH1* gene through epigenetic silencing. Overall, MSI-H tumors account for 23-30% of ECs (both sporadic and Lynch-related) (10-13). LS accounts for 2-6% of ECs overall and 30% of MSI-H ECs are secondary to LS (4, 13, 14)

The clinical relevance of MSI status has recently been recognized, as MSI-H colon and gastric tumors have shown an overall survival advantage over microsatellite stable (MSS) tumors (15, 16). In colon cancer, this survival benefit is limited to those patients not receiving adjuvant chemotherapy (17). Several studies have shown that adjuvant 5-fluorouracil is associated with improvement in overall survival in only MSS tumors and not MSI-H, and demonstrates the use of MSI as a marker of non-response to therapy (17, 18). However, it is not clear whether MSI-H ECs, including Lynch-related ECs, demonstrate this same survival benefit or whether it may be used as biomarker for therapy (19-21). Identifying a treatment targeting this molecular subgroup of EC could help to improve responses in some recurrent and advanced cases.

TREATMENT OF ADVANCED ENDOMETRIAL CANCER

For those patients with advanced and recurrent EC that fail treatment with standard chemotherapy, response to subsequent chemotherapy is poor, and attempts to identify promising targeted agents have been limited. Combination chemotherapy in advanced cases has response rates (RR) of 40-60%, and decreases further to 9-30% if initial therapy

is unsuccessful (22-24). Those with recurrent EC that are not candidates for radiation therapy also have similar responses to combination chemotherapy. In order to improve RR, attempts to identify drugs that target specific molecular alterations have been made, but with very limited success. As previously shown and then confirmed in the TCGA, EC has frequent phosphatase and tensin homolog (*PTEN*) mutations and aberrant regulation of the phosphatidylinositol 3-kinase (PI3K)/Akt/mammalian target of rapamycin (mTOR) signaling pathway. This pathway has been targeted with mTOR inhibitors in those with recurrent and metastatic EC and shown partial responses of 9-14% and stable disease ranging from 40-70% (25-27). However, no complete responses have been demonstrated. Additionally, limited success of less than 15% RR has been seen with other targeted agents, thus far (28, 29). As of now, no recommended targeted therapies exist for EC despite attempts to identify subgroups that would benefit from such therapy.

CANCER IMMUNOTHERAPY

Immunotherapy has recently emerged as a promising treatment strategy in multiple tumor subtypes and could improve treatment outcomes in advanced and recurrent EC. Tumors demonstrating increased tumor immunogenicity are particularly good candidates for this type of treatment. The tumor specific somatic mutational rate is thought to correlate with the number of tumor specific neoantigens produced, based on prediction models (30). These neoantigens are then recognized by the immune system as non-self and can trigger an anti-tumoral immune response with immune cell infiltration into these tumors and cytotoxic T lymphocyte (CTL) activation (30). The ability to then harness and amplify this anti-tumor immune response is the basis of cancer immunotherapy.

Mounting an Anti-Tumor Immune Response

Tumor infiltrating lymphocytes (TILs), including CTLs, have been recognized as a key indicator of anti-tumor immune response. In fact, CTLs are the major effectors of the adaptive anti-tumor immune response. Naïve $CD8^+$ T cells are transformed into CTLs through T cell receptor (TCR) recognition of antigen presentation by major histocompatibility (MHC) class I molecules. This activation also requires co-stimulation by the T cell associated receptor CD28 binding to either the CD80 or CD86 ligand on the antigen presenting cell (31). CTLs then direct specific anti-tumor activity through the release of cytoloytic granules, such as granzyme B and perforin. This was initially supported in part by the association of TILs and CTLs with improved survival in multiple tumor types (32-34). While the field of cancer immunotherapy has grown exponentially in recent years, few studies have focused specifically on endometrial cancer. As a result, our understanding of mechanisms of immunotherapy must borrow heavily from other tumor types.

However, CTLs are not the only cells that participate in anti-tumor immune response. Many different immune cell populations are involved in both the anti-tumor and immune evasion responses. Natural killer (NK) cells are a component of the innate immune response and, like CTLs, also have directed cytolytic activity against tumor cells (35). $CD4^+$ T helper cells, in contrast, contribute to the anti-tumor response by enhancing activation of CTLs, as well as, NK cells and macrophages (36). Successful cancer immunotherapy requires tipping the balance to favor anti-tumor response while blocking mechanisms of tumor evasion. A summary of the immune cells and corresponding receptors evaluated in this thesis is depicted in table 1.

Table 1. Common immune cells and immune cell markers seen in the tumor immune microenvironment.

Immune Cell	Function	Markers
T cell	Lymphocyte that participates in cell mediated immunity and adaptive immune response	General: CD3
$CD8^+$ T cell	T lymphocyte that participates in the adaptive immune response with tumor directed killing after transformation to CTL	General: CD3, CD8 Activated: Granzyme B Intraepithelial: CD103
Helper T cell	Specific T cell that participates in the adaptive immune response through cytokine release which activates B cells, T cells, macrophages, and NK cells	General: CD3, CD4
Natural Killer Cell	Cytotoxic lymphocyte that participates in the innate immune response	General: NKp46 Activated: Granzyme B
Macrophage	Antigen presenting cell and phagocyte	General: CD68
Dendritic Cell	Antigen presenting cell	General: CD11c

Mechanisms of Tumor Evasion

Despite the presence of CTLs in tumors with increased immunogenicity and tumor directed immune activation, these tumors are still capable of evading the immune response. Tumor associated macrophages (TAMs) are thought to play a critical role in the development of immune evasion. These macrophages are induced by cytokines in the tumor microenvironment (IL-10 and IL-4) to undergo transformation into type II macrophages (37). This specific macrophage subset has limited antigen presenting capacity and instead suppresses T cell function, thus creating a pro-tumorigenic environment (37). $CD4^+$ T cells can also be transformed into T regulatory cells which

have immunosuppressive activity, that is in contrast to the T helper cell function mentioned previously (38).

Immune evasion is also attributed to upregulation of immune checkpoints on immune cells that work to dampen the immune response. Normally this pathway helps to prevent autoimmune tissue destruction; however, the tumor microenvironment hijacks this immune regulation to prevent ongoing tumor directed immune attack. The most common immune checkpoints expressed are CTLA-4 (cytotoxic T lymphocyte associated protein 4) and PD-1 (programmed death 1). Both CTLA-4 and PD-1 function in distinct biological pathways and demonstrate different patterns of expression (39). Figure 3 summarizes the CTLA-4 and PD-1 immune cell inhibitor action. The CTLA-4 receptor is expressed immediately upon T cell activation, and then competitively binds the T-cell co-stimulatory signal (CD80 and CD86), to reduce the magnitude of the immune response. PD-1 receptor expression, in contrast, is delayed as it requires gene transcription. The PD-1 inhibitor pathway also acts more locally within the tumor microenvironment as the ligand for PD-1 (PD-L1) can be expressed by both tumor and infiltrating immune cells (39). Upregulation of PD-L1 expression by both the tumor and infiltrating immune cells is another adaptation for immune evasion (40). In fact, PD-L1 expression has been shown to be upregulated in tumor cells that are immediately adjacent to TILs and it has been suggested that TILs induce their own inhibition through cytokine release that result in upregulation of PD-L1 (40).

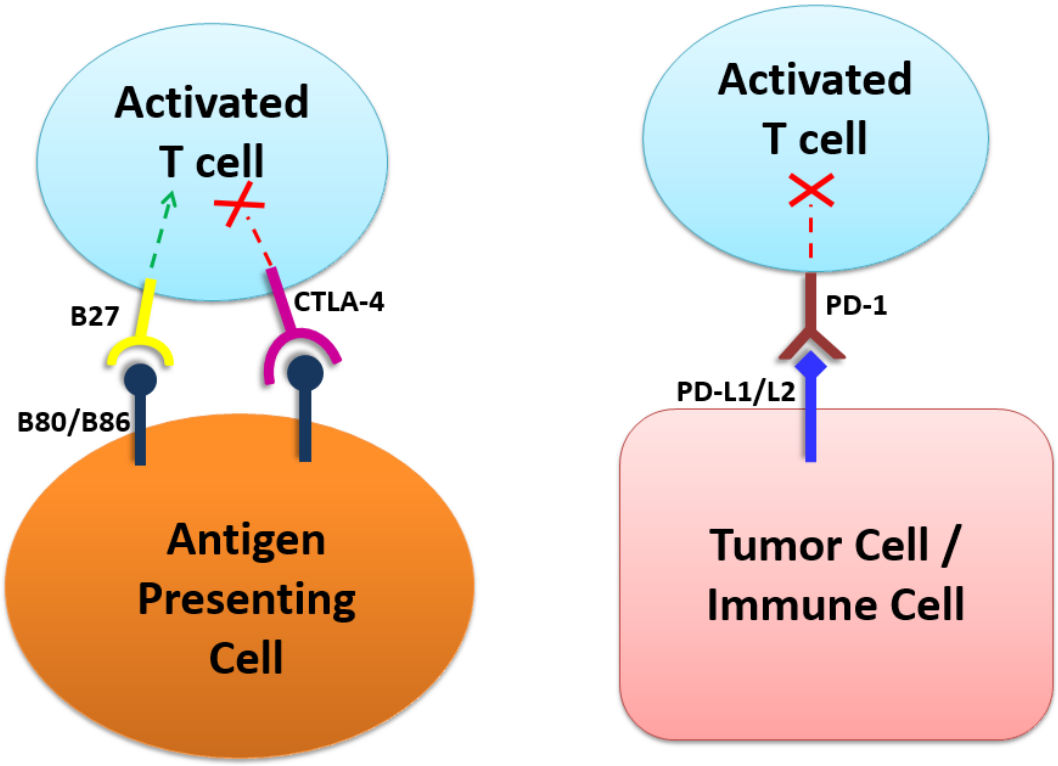

Figure 2. Immune checkpoints help to regulate immune responses and can be utilized by the tumor microenvironment to dampen and inhibit tumor directed immune responses.

CTLA-4 and PD-1 are commonly expressed immune checkpoints. B27 is expressed by T cells and binds CD80 and CD86 as a co-stimulatory signal to T cell antigen recognition. CTLA-4 is also expressed by activated T cells and competitively binds the T cell co-stimulatory ligands CD80 and CD86 leading to deamplification of the immune response. Additionally, the PD-1 receptor expression by T cells acts within the tumor microenvironment to inhibit the immune response. It binds PD-L1 and PD-L2 expressed by both the tumor and other immune cells.

Expression of Immunotherapy Targets

Expression of PD-L1 differs among tumor types, and remains an area of continued investigation. A summary of the PD-L1 expression studies discussed below can be found in Table 2. In a study by Taube et al, PD-L1^{+} tumors were defined as those with at least 5% tumoral expression and expression was characterized across tumor types. This study

showed a wide range of expression, with castration-resistant prostate cancers (CRPC) having no PD-L1$^+$ cases compared to 90% positivity of kidney cancers (41). Additionally, about 50% of melanoma and non-small cell lung cancer (NSCLC) cases were PD-L1$^+$. This same study also found positive expression of PD-L1 on infiltrating immune cells in half of melanomas, NSCLCs, and colorectal cancers (CRC). Another study evaluating pretreatment PD-L1 expression found PD-L1 expression in several tumor types to be more common on infiltrating immune cells than on the tumor cells themselves (42). The percentage of PD-L1$^+$ tumor cells ranged from 1% (CRC) to 24% (NSCLC). In contrast, the percentage of PD-L1$^+$ immune cells ranged from 12% (pancreatic cancer) to 36% (melanoma).

Monoclonal antibodies against both CTLA-4 and PD-1, as well as against PD-L1, have shown efficacy in multiple cancer types, however, the potential value of PD-L1 expression as biomarker for response is still uncertain (43-45). In a study of nivolumab (anti-PD-1 antibody) across tumor types, objective response was correlated with tumoral PD-L1 expression but not PD-L1 expression by infiltrating immune cells (41). Treatment with MPDL3280A (anti-PD-L1 antibody) has also demonstrated objective responses of 13-26% among a variety of different malignancies (42). Although the RR alone was not overly impressive in this study, the majority of responders had durable responses lasting at least one year. In contrast to nivolumab treatment, response to MPDL3280A was significantly correlated with PD-L1 expression on immune cells rather than tumoral PD-L1 expression. Given this early conflicting data that may reflect the differences in the immune microenvironment among tumor types, the use of PD-L1 expression as a biomarker for response to immune checkpoint inhibiting agents requires additional investigation.

Table 2. Immunotherapy literature summary

PD-L1 Studies					
Author(y)	**Cancer Type**	**Marker**	**PD-L1 Expression**	**Findings**	**Ref**
Taube (2014)	Melanoma NSCLC Colorectal CRPC	PD-L1$^+$ tumor or immune cells (≥5% of cells)	Tumor Cells Melanoma (47%) NSCLC (53%) Colorectal (13%) CRPC (0%) Immune Cells Melanoma (50%) NSCLC (53%) Colorectal (50%) CRPC (0%)	**Treatment with nivolumab (anti-PD1)** -PD-L1$^+$ tumor cells associated with ORR (p=0.03) and clinical benefit (p=0.01). -PD-L1$^+$ immune cells associated only with clinical benefit (p=0.04)	41
Herbst (2014)	Melanoma NSCLC Colorectal Renal Cell Head and Neck	PD-L1$^+$ tumor or immune cells (≥5% of cells)	Tumor Cells Melanoma (5%) NSCLC (24%) Colorectal (1%) Renal Cell (10%) Head and Neck (19%) Immune Cells Melanoma (36%) NSCLC (26%) Colorectal (35%) Renal Cell (25%) Head and Neck (28%)	**Treatment with MPDL3280A (anti-PD-L1)** -PD-L1$^+$ immune cells associated with response to treatment (p=0.01) -PD-L1$^+$ tumor cells not associated with response (p=0.08)	42

Abbreviations: NSCLC, non-small cell lung cancer; CRPC, castration-resistant prostate cancer; overall response rate, ORR

CD8$^+$ T Cell Subpopulations

In addition to the presence of TILs, CTLs, and immune checkpoint expression, other CD8$^+$ T cell subpopulations have been investigated and associated with improved survival and tumor immunogenicity. In high grade serous ovarian cancer (HGSOC), the presence of CD8$^+$ T cells within the tumor epithelium has been associated with improved prognosis (46). Retention of these CD8$^+$ T cells to the tumor epithelium is thought to be mediated by expression of CD103 (α_E/β_7 integrin) on the T cell which binds to E-cadherin in the tumor epithelium (47). Furthermore, high prevalence of CD8$^+$CD103$^+$ T cells in HGSOC correlates with enhanced survival (48). This interaction of CD103 with the E-

cadherin ligand has also been proposed as a mechanism for tumor specific recognition by CTLs (49).

IMMUNOTHERAPY IN MSI-H TUMORS

Some MSI-H tumor types, have been reported to be more immunogenic and also demonstrated increased expression of immune checkpoints. MSI-H CRCs have a higher density of TILs and CTLs and increased immune checkpoint expression compared to MSS colorectal cancers (50, 51). Specifically, Llosa et al. showed MSI-H CRCs have increased CTL infiltration and activation within the epithelial component of the tumor, the tumor-associated stroma, and at the invasive front (50). Along with this pro-inflammatory environment, expression of multiple immune checkpoint markers were also increased in MSI-H colorectal cancers, including PD-1, PD-L1 , CTLA-4 , LAG-3 (lymphocyte-activation gene 3), and IDO (Indoleamine 2,3-dioxygenase). It is suggested that the presence of CTLs and increased immune checkpoint expression in tumors are key indicators that immunotherapy may have increased efficacy in MSI-H tumors.

Due to these reports of enhanced immunogenicity, the efficacy of immunotherapy in MSI-H tumors is now being evaluated in clinical studies. Specifically, the observation of increased immune checkpoint expression in colorectal MSI-H tumors has led to trials of immune checkpoint blockade. Pembrolizumab, a monoclonal antibody targeting PD-1, was recently studied in a phase 2 trial of progressive and metastatic MSI-H CRC. This trial showed improved immune-related objective response rates (encompasses patterns of response specific to immunotherapy) in MSI-H CRC compared to MSS CRC (52). Of interest, a third arm of the study included patients with MSI-H non-CRC tumors, including two women with EC, and also demonstrated improved response to anti-PD-1 therapy. Of

the two EC patients, one had a complete response and the other a partial response to anti-PD-1 therapy. Updates to this study, with the inclusion of additional MSI-H EC patients, were recently presented at the 2016 Society of Gynecologic Oncology Annual Meeting (53). Response rates of 56% were seen in the MSI-H EC population (n=9), including one complete response and four partial responses, and additional studies in MSI-H and MSS ECs are currently being planned.

IMMUNE MICROENVIRONMENT OF MSI-H ENDOMETRIAL CANCER

While our knowledge of the immune microenvironment in cancer has grown overall, our understanding in EC has lagged behind. A few studies have evaluated the relationship of the immune microenvironment and survival in EC. Kondratiev et al, demonstrated an association with improved overall survival for patients with tumors containing at least 10 $CD8^+$ T cells at the invasive front (54). Higher numbers of TAMs are also found in the stroma compared to the tumor epithelium in EC overall, but has not been associated with tumor stage or disease status (55).

A small number of limited studies have shown conflicting data regarding the immune microenvironment and immunogenicity of MSI-H EC and these studies have not addressed Lynch-related cases specifically (56-58). One recent study by Howitt et al predicted the neoantigen load of MSI-H EC to be 7-fold higher compared MSS EC using TCGA data (56). Additionally, this study used immunohistochemistry to characterize further parameters of the immune microenvironment. However, it is important to note that the number of cases used in this study was small and immunohistochemistry evaluation was limited to one high powered field per case. Yet, this limited study found a significantly higher number of $CD3^+$ and $CD8^+$ TILs in MSI-H and POLE compared to MSS ECs.

Lastly, PD-L1 expression on immune cells of the MSI-H/POLE tumors was higher than in MSS, but there was no difference in tumoral PD-L1 expression. Another study by van Gool et al, also showed higher $CD8^+$ T cell infiltration in both the intraepithelial and intrastromal regions of MSI-H compared to MSS tumors (59). This same study also evaluated immune gene expression using TCGA and found increased CD8A and IFNγ expression in MSI-H tumors, but no significant difference in perforin or granzyme B expression.

These early studies offer hints that the immune microenvironment of MSI-H ECs may be similar to that seen in MSI-H CRC with increased immunogenicity and immune cell infiltration. However, the specifics of the immune environment of MSI-H EC and how this may differ from MSS EC still remain largely unknown. Therefore, there is a *critical need* to understand the immune microenvironment of MSI-H EC to determine if this subtype is amenable to treatment with immunotherapy. It is also unknown if Lynch syndrome-related MSI-H (LS MSI-H) ECs have a comparable immune microenvironment to sporadic MSI-H EC. Our central hypothesis is that MSI-H ECs will have an altered immune microenvironment compared to MSS ECs, and demonstrate increased immune checkpoint expression. To address this question we first used TCGA uterine data to evaluate differences in gene expression and global pathway alterations between MSI-H and MSS ECs. We then performed immunohistochemistry (IHC) multiplexing with advanced quantitation methods to further characterize the differences in immunologic markers between these tumor types.

Chapter 2: Methods

TCGA Analysis

In collaboration with the Bioinformatics Resource Group at The University of Texas MD Anderson Cancer Center, TCGA uterine cancer RNA sequencing (RNAseq) version 2 dataset was used to evaluate gene expression differences between MSI-H and MSS EC. From this data, 118 MSI-H cases and 160 MSS cases were identified and used for the analysis. RNAseq read counts were converted into integer values via rounding in Excel. Genes with a median read count of less than 10 for both groups were filtered out. This left 15393 genes out of an initial 20531 genes for evaluation. Next, significance analysis of microarrays (SAM) (Stanford University, CA) was used to detect statistically significant differences in gene expression between the two groups as two class, unpaired samples. Only genes with a q value < 0.05 were extracted for further pathway evaluation. The false discovery rate was accounted for by using the q value that signifies that 5% of significant results will result in false positives.

Ingenuity Pathway Analysis (IPA) (Qiagen, CA) was then used to investigate pathway alterations between MSI-H and MSS EC. The differentially expressed genes obtained from SAM analysis, as described above, were uploaded to IPA to create a Core Analysis, which was used to investigate differences in canonical pathways in MSI-H versus MSS tumors.

A more specific TCGA analysis focused on immune-related and inflammatory genes was later conducted with recently released updated Level 3 uterine cancer data. In Level 3 expression data, gene and mRNA levels RNAseq data is post normalization and processed to allow for interpretive analysis (60). This particular analysis evaluated mRNA

level differences in a more specific immune and inflammatory gene panel as described by Lal et al (61). The list of queried genes can be seen in Table 3.

Table 3. Immune related genes investigated with TCGA uterine data

Gene ID	Gene Name
ACTB	Beta actin
CCL11	Chemokine ligand 11
CCL2	Chemokine ligand 2
CCL5	Chemokine ligand 5
CD247	CD247 molecule
CD274	CD274 molecule
CD276	CD276 molecule
CD3D	CD3d molecule, delta
CD3E	CD3e molecule, epsilon
CD3G	CD3g molecule, gamma
CD4	CD4 molecule
CD80	CD80 molecule
CD86	CD86 molecule
CD8A	CD8a molecule
CD8B	CD8b molecule
CTLA4	Cytotoxic T-lymphocyte associated protein 4
CX3CL	Chemokine ligand 1
CXCL10	Chemokine ligand 10
CXCL9	Chemokine ligand 9
FOXP3	Forkhead box P3
GNLY	Granulysin
GZMB	Granyzme B
HLA-A	Major histocompatibility complex, class I, A
HLA-B	Major histocompatibility complex, class I, B
HLA-C	Major histocompatibility complex, class I, C
HLA-DMA	Major histocompatibility complex, class II, DM alpha
HLA-DMB	Major histocompatibility complex, class II, DM beta
HLA-DOA	Major histocompatibility complex, class II, DO alpha
HLA-DOB	Major histocompatibility complex, class II, DO beta
HLA-DPA1	Major histocompatibility complex, class II, DP alpha 1
HLA-DPB1	Major histocompatibility complex, class II, DP beta 1
HLA-DQA1	Major histocompatibility complex, class II, DQ alpha 1
HLA-DQA2	Major histocompatibility complex, class II, DQ beta1
HLA-DRA	Major histocompatibility complex, class II, DR alpha
HLA-DRB5	Major histocompatibility complex, class II, DR beta 5
ICAM1	Intercellular adhesion molecule 1
ICOS	Inducible T cell co-stimulator
IFNG	Interferon gamma
IL10	Interleukin 10
IL12RB2	Interleukin 12 receptor, beta 2
IL17A	Interleukin 17A

Gene ID	Gene Name
IL18RAP	Interleukin 18 receptor accessory protein
IL7R	Interleukin 7 receptor
IRF1	Interferon regulatory factor 1
KLRK1	Killer cell lectin-line receptor subfamily K, member 1
LAG3	Lymphocyte-activation gene 3
MADCAM1	Mucosal vascular addressin cell adhesion molecule 1
MICB	MHC class I polypeptide-related sequence B
PDCD1	Programmed cell death 1
PDCD1LG2	Programmed cell death 1 ligand 2
PROCR	Protein C receptor, endothelial
RAET1E	Retinoic acid early transcript 1E
RAET1G	Retinoic acid early transcript 1G
STAT1	Signal transducer and activator of transcription 1
STAT3	Signal transducer and activator of transcription 2
TBX21	T-box 21
TNFRSF14	Tumor necrosis factor receptor superfamily, member 14
TNFSF4	Tumor necrosis factor superfamily, member 4
ULBP1	UL16 binding protein 1
ULPB2	UL16 binding protein 2
ULPB3	UL16 binding protein 3
VCAM1	Vascular cell adhesion molecule 1
VTCN1	V-set domain containing T cell activation inhibitor 1

REAGENTS AND ANTIBODIES

The Opal™ IHC kit (PerkinElmer, MA) was used for fluorescent IHC multiplexing. The kit included fluorescent tyramide signal amplification (TSA) reagents, amplification diluent, and DAPI (4',6-diamidino-2-phenylindole).

The following antibodies were used for fluorescent IHC multiplexing: CD3 (1:900, clone SP7, Thermo Scientific, MA), CD4 (1:450, clone 4B12, Thermo Scientific, MA), CD8 (1:400, clone 4B11, Leica, UK), CD11c (1:1000, clone 5D11, Leica, UK), Granzyme B (1:300, clone 11F1, Leica, UK), CD103 (1:5000, clone EPR4166, Abcam, MA), CD68 (1:500, clone KP1, Biogenex, CA), PD-L1 (1:1600, clone E1L3N, Cell Signaling, MA), and NKp46 (1:4000, clone aa55-104, Lifespan Biosciences, WA).

Antibody diluent was used for antibody dilution (Invitrogen, CA). 10% normal goat serum blocking solution was used for background slide blocking (Life Technologies, CA). Citrate buffer of pH 6.0 was used for antigen retrieval (Poly Scientific, NY). Secondary anti-mouse or anti-rabbit antibody horseradish peroxidase (HRP) polymer conjugate was used prior to fluorophore application (Invitrogen, CA). Coverslips were mounted to slides with aqueous mounting solution (Thermo Scientific, MA)

TUMOR SPECIMENS AND CLINICAL DATA

Endometrial cancer specimens were identified from the gynecologic oncology archived tumor bank and Lynch syndrome patient registry in accordance with Institutional Review Board (IRB) protocols. In total, 59 MSI-H EC specimens were identified from 2000-2015. The majority of cases were from 2012-2015, but this time frame was expanding to include additional cases from the Lynch syndrome patient registry given the rarity of these tumors and the need for available primary tumor specimens. These cases were then matched approximately 1:2 to MSS cases; resulting in identification of 108 MSS cases. Matching was done according to histology, tumor grade, tumor stage, age at diagnosis, and body mass index (BMI) at time of diagnosis, as available. Clinical data for the cohort was abstracted from the medical record. Of the cases identified, nine specimens were unable to be located. When the missing specimen was an MSI-H case, its corresponding matched MSS cases were also filtered out from the dataset. If no MSS cases were found for any one MSI-H case, the MSI-H case was also removed from the dataset. Archived formalin-fixed paraffin embedded (FFPE) tumors were cut into 4 micron sections by the research histology core.

DETERMINATION OF MSI STATUS AND MMR DEFECT

MSI Testing

MSI status was determined clinically by a method developed by the Molecular Diagnostic Laboratory at MD Anderson Cancer Center (MDACC) that has been previously described (62). This data was reported in the medical record and collected retrospectively. Briefly, MSI testing was performed following extraction of DNA from FFPE tumor and normal tissue. A polymerase chain reaction (PCR) based method was used for analysis followed by capillary electrophoretic detection of microsatellite markers. Seven microsatellite markers were used in this method. These markers included BAT 25, BAT 26, BAT 40, D2S123, D5S346, D17S250, and TGFBR2. The number of tumor microsatellite repeats for each of the markers was compared to normal tissue from the same case. A tumor was considered to have microsatellite instability if three or more of the seven markers demonstrated allelic shift.

DNA MMR Deficiency by IHC

The process for identification of DNA MMR deficiency was developed by the Molecular Diagnostic Laboratory at MDACC as previously described (62), and the information was collected retrospectively from the pathology report. Immunohistochemistry was performed on FFPE tumor blocks to assess expression of MMR proteins (MLH1, MSH2, MSH6, PMS2). Lack of protein expression of MSH2, MSH6, or PMS2 in the tumor, by this method, was considered probable Lynch syndrome. For those with MLH1 loss by IHC, MLH1 promoter methylation was performed. Those cases showing MLH1 loss by IHC and without MLH1 promoter methylation were

classified as probable Lynch syndrome. IHC was used to define probable Lynch syndrome as germline MMR gene mutation testing was not available on all case.

Promoter Methylation

MLH1 promoter methylation status was also determined via a method developed by the MDACC Molecular Diagnostic Laboratory and collected retrospectively from the pathology reports in the electronic medical record. Briefly, bisulfate was used to treat extracted DNA from FFPE samples. This resulted in conversion of cytosine to uracil in unmethylated cases. PCR amplification of methylated and unmethylated MLH1 promoter region was performed and these sequences were labeled fluorescently and detected via capillary electrophoresis as previously described (63).

IMMUNOHISTOCHEMISTRY STAINING

Antibody Optimization

Prior to initiation of IHC multiplexing, each antibody of interest was tested to determine optimal antibody dilution and antigen retrieval (AR) temperature. A set of serial dilutions for each antibody was performed based on published IHC data and the manufactures recommendations to establish the best dilution and AR temperature.

Multiplexing

Multiple panels were required to enable evaluation of nine total markers. Some markers were repeated on multiple panels to allow for colocalization studies. The individual panels are described in detail below. Details of the IHC multiplexing protocol follow the multiplexing panel descriptions.

Multiplexing (6-plex) Panel #1

For the first IHC multiplexing panel, the following antibodies were used: anti-Granzyme B for activated CTLs and NK cells, anti-CD8 for $CD8^+$ T cells, anti-NKp46 for NK cells, anti-CD68 for macrophages, anti-PD-L1 for PD-L1 expressing cells, and DAPI. The order of antibody application and associated fluorescent TSA reagent was as follows: (1) anti-Granzyme B/Cyanine 3 (Cy3), (2) anti-CD8/Fluorescein (FITC), (3) anti-CD68/Cyanine 5.5 (Cy5.5), (4) anti-PD-L1/Cyanine 3.5 (Cy3.5), (5) anti-NKp46/Cyanine 5 (Cy5), and (6) DAPI. The staining sequence is also represented in Table 4 along with the specific antibody dilution and manufacturer.

Multiplexing (5-plex) Panel #2

For the second multiplexing panel, a slightly modified set of reagents had been updated by the manufacturer. The new fluorescent TSA reagents had undergone further stringent evaluation and optimization by the manufacturer for IHC multiplexing use; however, all IHC processing steps remained the same. Names of the new fluorophores (shown below and in Table 4) reflect the excitation wavelength in nanometers (nm). The following antibodies were used for this multiplexing set: anti-CD3 for all T cells, anti-CD4 for helper T cells, anti-PD-L1 for PD-L1 expressing cells, and anti-CD11c for dendritic cells. The order of antibody application and associated fluorescent TSA reagent was as follows: (1) anti-CD3/520 nm, (2) anti-CD4/540 nm, (3) anti-PD-L1/620 nm, (4) anti-CDllc/690 nm, and (5) DAPI.

Multiplexing (3-plex) Panel #3

Antibodies for this set included: anti-CD8 for $CD8^+$ T cells and anti-CD103 for intraepithelial T cells. The order of antibody application and associated fluorescent TSA

reagent was as follows: (1) anti-CD103/520 nm, (2) anti-CD8/620 nm, and (3) DAPI. Table 4 contains the specific antibody conditions and staining sequence.

Table 4. Fluorescent IHC multiplexing antibodies and conditions.

Primary Antibody	Company	Host	Conc.	AR Temp (°C)	TSA	Order
Multiplexing Panel #1						
Granzyme B	Leica	mouse	1:300	96	Cy3	1
CD8	Leica	mouse	1:400	96	FITC	2
CD68	Biogenex	mouse	1:500	120	Cy5.5	3
PD-L1	Cell Signaling	rabbit	1:1600	96	Cy3.5	4
NKp46	Lifespan Biosciences	rabbit	1:4000	120	Cy5	5
DAPI						6
Multiplexing Panel #2						
CD3	Thermo Scientific	rabbit	1:900	96	520	1
CD4	Thermo Scientific	mouse	1:450	96	540	2
PD-L1	Cell Signaling	rabbit	1:1600	96	620	3
CD11c	Leica	mouse	1:1000	96	690	4
DAPI						5
Multiplexing Panel #3						
CD103	Abcam	rabbit	1:5000	96	520	1
CD8	Leica	mouse	1:400	96	620	2
DAPI						3

Abbreviations: Conc, concentration; AR, antigen retrieval; TSA tyramide signal amplification.

.

Immunohistochemistry Protocol

The Opal™ fluorescent multiplexing kit from Perkin Elmer (Waltham, MA) was used according to the manufacturer's protocol as previously described by Stack et al (64).

Details are given below and a flow chart of the steps can also be seen in Figure 3. Antibody details including dilutions, manufacturers, and AR conditions are shown in Table 4.

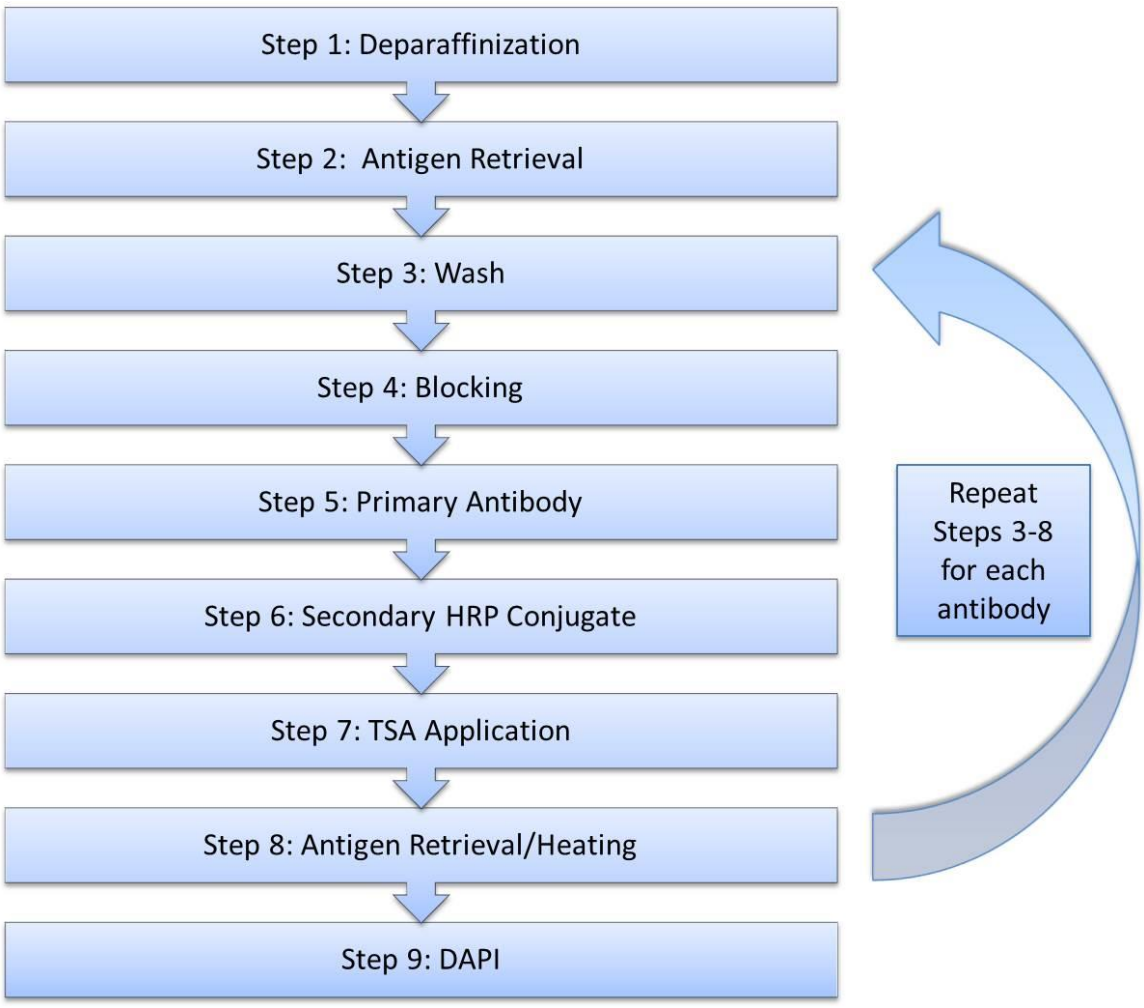

Figure 3. Flow chart of fluorescent IHC multiplexing method.

STEP 1: DEPARAFFINIZATION

Deparaffinization was performed by submerging slides into three successive containers of xylene for 10 minutes each. A series of ethanol solutions was then used to rehydrate the tissue as follows: 100% for five minutes, 95% for five minutes, and 70% for

two minutes. Following rehydration, the slides were washed in distilled water (dH2O) for two minutes then in Tris-Buffered Saline with 0.05% Tween 20 (TBST) for two minutes. After deparaffinization, care was taken to ensure slides were kept in light blocking containers throughout the remaining IHC process to limit unnecessary light exposure.

Step 2: Antigen Retrieval

Next, AR was carried out by placing the slides in citrate buffer (pH 6.0) and heating the slides via a decloaking chamber for 15 minutes. The set temperature for AR was determined based on laboratory optimization and antibody manufacturers' recommendations.

Step 3: Wash

After heating was completed, the slides were removed from the decloaking chamber and cooled for 20-30 minutes to room temperature. The slides were then washed in dH2O for two minutes followed by TBST for two minutes. For the NKp46 antibody, an additional wash of 1% hydrogen peroxide for 10 minutes followed by a TBST was for two minutes was used to decrease endogenous peroxidase activity. This step was not required for any of the other antibodies.

Step 4: Blocking

Slides were then removed from the wash solution. Excess liquid was wiped from the slides and the tissue was demarcated using a hydrophobic barrier pen. Sufficient 10% normal goat serum (Life Technologies, CA) blocking solution was applied to cover the tissue (75-100 microliters (μL)) and slides were incubated in a humidified chamber.

STEP 5: PRIMARY ANTIBODY

After 30 minutes, the blocking solution was removed from the slides and primary antibody was applied to the tissue. Again, sufficient diluted antibody solution (75-100 μL) was used to cover the tissue. Slides incubated with the primary antibody in a humidified chamber at 4°C overnight. For the anti-CD103 antibody, the slides were incubated at room temperature for 30 minutes in a humidified chamber before proceeding with washing as described below. All other antibodies used the overnight incubation procedure.

After overnight incubation (approximately 16 hours), primary antibody was removed from the slides. The slides were then washed in TBST with agitation and at room temperature for two minutes. This wash process was repeated three times.

STEP 6: SECONDARY HRP CONJUGATE

Slides were wiped of excess liquid and 100 μL of diluted secondary HRP conjugate (Invitrogen, CA) was applied to the tissue. Depending on the host species of the primary antibody, either mouse or rabbit secondary HRP conjugate was used. Slides were incubated in a humidified chamber at room temperature for 10 minutes. The slides were again washed three times in TBST with agitation at room temperature for two minutes.

STEP 7: TSA APPLICATION

The fluorophore labeled TSA reagent was first resuspended in 150 μL of dimethyl sulfoxide (DMSO) and then diluted 1:50 in 1X Amplification Diluent (Perkin Elmer, MA) to produce the working TSA solution. Slides were wiped of excess liquid and 75-100 μL of TSA working solution (Perkin Elmer, MA) was applied to the tissue. The slides were incubated in a humidified chamber at room temperature with the TSA solution for 10

minutes. The slides were again washed in TBST for two minutes at room temperature three times. A different fluorophore labeled TSA solution was used for each antibody.

STEP 8: ANTIGEN RETRIEVAL/HEATING

Slides were again heated in citrate buffer of pH 6.0 for 15 minutes in a decloaking chamber. Following heating, the slides were left to cool to room temperature for 20-30 minutes in the citrate buffer. The slides were then washed with dH20 for two minutes, followed by TBST for two minutes at room temperature. The specific temperature was determined by the conditions needed for AR of the next antibody to be applied. For the last heating step in the multiplexing sequence, 96°C was used.

After step 8, the process was repeated beginning at step 3 for each subsequent antibody used. After the final antibody and fluorophore labeled TSA solution was applied, the process proceeded to step 9.

STEP 9: DAPI

DAPI solution from the Opal™ fluorescent multiplexing kit (PerkinElmer, MA) was then applied. This solution was diluted two drops in one mL of TBST prior to application. 100 µL of the diluted DAPI solution was applied to the tissues and incubated in a humidified chamber at room temperature for five minutes. DAPI was then removed and the slides were washed in dH20 for two minutes. A drop of aqueous mounting solution (Thermo Scientific, CA) was applied to the slides for cover slip mounting. The slides were stored in a dark container at 4°C.

Control Slides

Individual fluorophore control slides were prepared for each antibody and associated fluorophore labeled TSA reagent in order to create a spectral library and to determine imaging exposure times for each fluorophore. This was accomplished using IHC steps 1-8 as described above. Similarly, a DAPI only slide was stained using the described IHC steps 1-3. DAPI was then applied as described in step 9. Lastly, an unstained slide of uterine tissue was deparaffinized and heated as above and mounted to be used for determination of autoflourescence during the imaging analysis process.

IMAGING AND DATA ANALYSIS

The imaging and inForm® analysis portion of the project was performed with assistance from the MDACC Flow Cytometry and Cellular Imaging Facility.

Imaging

Due to the multiple antibodies and multiple fluorophores used for several markers on each slide, unique imaging was required. This multispectral imaging was accomplished with the Vectra® 2 automated system (PerkinElmer, MA). This system allows for the capture of tissue images at multiple wavelengths and is able to analyze multiple markers, or antibodies, on a single slide. Analysis of multiple markers on a single slide also enables colocalization studies.

Initial low power images at 4X were obtained for all tissue on each slide. Up to 30 high power field images were then randomly captured at 20X through automation by the Vectra® system. These fields were captured based on highest density of tumor cells in the images. A series of sample EC multiplex images from the data set were used to define areas of tumor, stroma, and normal tissue that was then applied to create a pattern recognition algorithm for high power field acquisition. For the multiplexing sets, four

filters were used to capture images (DAPI, Cy3, FITC, and Cy5). Exposure times were determined for each of the filters using a representative individually stained slide, and subsequently used for acquisition of all images.

inForm® Analysis

Once images were obtained, the inForm® system version 2.1.5430.24864 was used to create a spectral library of each of the fluorophores. Images from the single fluorophore slides were used for this library. This allowed for unmixing of the individual fluorophores, and confirmed unique staining for each of the antibodies.

This same system was also used to identify tissue regions of interest and to score positive cellular tagging of the antibodies of interest. A series of multiplex images were randomly selected to provide a sample set of images to define areas of tumor epithelium, tumor associated stroma, myometrium and blank space. This sample set of images was then used to train the inForm® system in pattern recognition of these different tissue segments. The training algorithm also included DAPI and each spectral component, specific to the multiplex staining panel, to create the tissue segmentation algorithm that was applied to all images. The system was subsequently able to classify the pixels within the training set with 85-94% accuracy.

Next, DAPI staining was used to identify nuclei within each of the tissue compartments, and to obtain total cell counts with in each of the compartments. The DAPI staining was also used as a reference to determine cellular cytoplasm and membrane segmentation based on the inForm® algorithm. Thresholds and scoring for positively staining cells for each of the antibodies were determined through manual examination of each antibody among the EC multiplex training images. This examination included

identifying a fluorescent pixel intensity that accurately identified positive staining cells across the training set within the cellular compartment (cytoplasm or membrane) unique to each of the antibodies. Signal thresholds were determined using average fluorescent pixel density for each of the fluorophores and corresponding antibodies. Thresholds, along with cellular compartment of interest, are as follows:

- Multiplexing Panel #1: Granzyme B/Cy3 - membrane (score >3), CD8/FITC - membrane (score >2), PD-L1/Cy3.5 - cytoplasm (score >5), NKp46/Cy5 - membrane (score >1), and CD68/Cy5.5 – cytoplasm (score >1).
- Multiplexing Panel #2***:*** CD3/520 nm – membrane (score >0.83), CD4/540 nm - membrane (score >0.33), PD-L1/620 nm - cytoplasm (score >2.5), and CDllc/690 nm - membrane (score >0.2).
- Multiplexing Panel #3: CD103/520 nm – membrane (score >2.0) and CD8/620 nm - membrane (score >4.5).

For each antibody, signal greater than the determined threshold was considered positive staining.

An inForm® algorithm was then run based on the previously defined tissue segmentation, identification of individual cells and corresponding cellular compartments, and the scoring system for each of the antibodies of interest. The generated composite images were reviewed manually, and the reviewer was blinded to MSI status during this review. In the manual review, images that were determined to have inaccurate tissue segmentation were added to the training set of images to improve segmentation accuracy. However due to the wide variation of tissue architecture, 100% accuracy was unable to be obtained and those images that appeared to have gross segmentation inaccuracy were

excluded from the analysis. Overall, there were on average 16 images analyzed per specimen (range 1-35). A small subset of slides required reimagining due to poor identification of tissue and tumor by the automated system, and in these cases, more than 30 images were allowed in repeat image capture. This accounts for the increased number of images in two cases with greater than 30 images.

Some cases were not included in the overall analysis due to problems with tissue quality or imaging. This occurred because of tissue degradation (likely due to multiple rounds of heating from the multiplexing process), lack of tumor cells present in that section, or lack of tumor images captured by the automated system from inaccurate tissue segmentation for image acquisition. If the removed case was MSI-H, the corresponding MSS matched pairs were also removed. Additionally, if a MSS case that was removed resulted in no matched cases for a MSI-H case, the MSI-H case was also removed from the analysis.

The number of positive staining cells for each of the antibodies was determined per millimeter squared (mm^2) within the tumor epithelium and tumor associated stroma for each of the cases using code written in SAS version 9.2 (Cary, NC) by collaborator Gary Chisholm (Programmer/Analysis, Department of Gynecologic Oncology and Reproductive Medicine).

STATISTICAL ANALYSIS

Statistical analysis was performed using Stata version 14.1 (College Station, TX). The Mann-Whitney and Kruskal-Wallis tests were used to compare demographic data between the groups as indicated. For overall comparison of immune cellular markers

between MSI-H and matched MSS cases, the nonparametric Mann-Whitney test was used. The Mann-Whitney test was also used for comparison of sporadic MSI-H and matched MSS cases, as well as, MSI-H Lynch cases compared to MSS matches. A p value of < 0.05 was used to signify statistical significance. Box plots were also created to compare differences among mRNA levels, positive staining cell counts, and percent positive staining cells. The upper border of the box represents the third quartile, the lower border the first quartile, and the line the median. The whiskers are defined using the Tukey box plot method where they represent 1.5 times the upper and lower interquartile range.

Chapter 3: Results

TCGA Analysis

Using TCGA uterine cancer RNAseq data, global gene expression was compared for 118 MSI-H endometrioid endometrial cancers and 160 microsatellite stable tumors. Analysis of the differential gene expression revealed 2148 upregulated and 2645 downregulated genes in MSI-H tumors compared to MSS tumors. Further examination of global pathway alterations using IPA demonstrated significant activation of the granzyme B signaling pathway in MSI-H compared to MSS tumors ($p<0.01$), but not in other immune- or inflammatory-related pathways. Genes in the granzyme B pathway include but are not limited to: granzyme B, perforin, caspase 3, caspase 8, caspase 9, apoptotic peptidase activating factor, DNA fragmentation factor, endonuclease G, and cytochrome c. Upon cytotoxic cell activation, the granzyme B pathway triggers cellular apoptosis of target cells and increased pathway activation suggests increased CTL activity in MSI-H tumors.

A panel of specific immune- and inflammatory-related genes was also compared using TCGA RNAseq data. Of the 64 genes evaluated, mRNA levels in MSI-H tumors were significantly elevated for 11 genes ($p<0.01$). These genes included multiple T cell effector (*CD8a*, *ICOS*, *MICB*, *ULBP1*), T cell attractant chemokine (*CXCL9*), immune checkpoint (*LAG3*), NK cell effector (*ULBP2*, *ULBP3*), immune cytokine (*IFNG*), regulatory T cell (*FOXP3*), and beta actin (*ACTB*) genes. A subset of the significant mRNA comparisons between MSI-H and MSS EC is represented in Figure 4. MSI-H tumors also had significantly decreased mRNA levels of an eosinophil chemotactic cytokine gene (*CCL11*) ($p<0.01$).

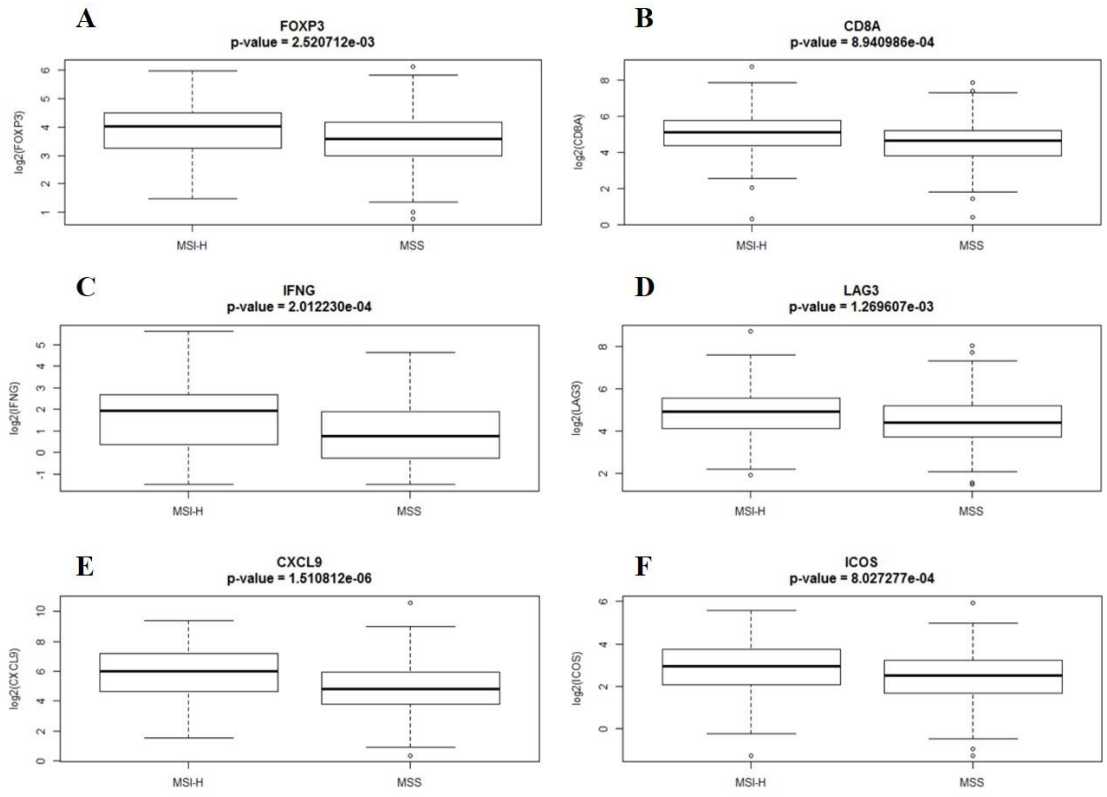

Figure 4. MSI-H ECs demonstrate increased expression of multiple T cell effector genes compared to MSS EC.

Analysis of RNAseq TCGA uterine cancer data comparing log2 mRNA level differences in MSI-H and MSS EC for **(A)** *FOXP3*, **(B)** *CD8A*, **(C)** *IFNG*, (D) *LAG3*, **(E)** *CXCL9*, and **(F)** *ICOS* represented by box plots.

SPECIMENS

Analysis of EC cases was conducted using specimens from the gynecologic oncology archived tumor bank and Lynch syndrome patient registry. In total, 59 MSI-H cases were identified and matched approximately 1:2 to 108 MSS cases. Of the MSI-H cases, 20 were found to have IHC defects in MMR genes consistent with probable Lynch syndrome and this group was used for the LS MSI-H sub-analysis. 37 MSI-H cases

demonstrated sporadic promoter methylation of MLH1 and were used for the sporadic MSI-H sub-analysis. One case had loss of MSH2 and MSH6 on IHC, but no germline deleterious mutations of DNA MMR genes. One case had unknown specific protein loss, but was positive for microsatellite instability with allelic shift in 5 of 7 microsatellite markers. These last two cases were included only in the overall MSI-H versus MSS analysis. Among the 20 LS MSI-H cases, IHC loss of primary MMR proteins were as follows: 3 (15.0%) in *MLH1*, 14 (70.0%) in *MSH2*, 3 (15.0%) in *MSH6*, and no cases showed loss of *PMS2* or *EPCAM*.

DEMOGRAPHICS

There were no significant differences in characteristics used for case matching (histology, age at diagnosis, BMI, stage, and grade) as shown in Table 5. Some data could not be obtained for a small number of cases in the MSI-H cohort, almost exclusively Lynch Syndrome EC cases. The majority of these cases were obtained from a Lynch syndrome patient registry where specimens included those collected from outside institutions, which had more limited associated clinical information. Of these, 11 cases were missing details of depth of myometrial invasion and 12 were missing LVSI information. As comparison of depth of invasion and LVSI were not primary objectives, and these cases were not excluded from the cohort. In addition, 2 cases had unknown grade (both LS MSI-H) and 5 had unknown stage (All LS MSI-H). However, these cases were matched according to the data available and were included in the analysis given the limited number of cases of the LS MSI-H subtype.

The majority of cases were stage IA in both groups (MSI-H 59.3% vs MSS 66.7%; p=0.80) with about 13% representing more advanced stage III or IV cases (MSI-H 13.6%

vs MSS 13.0%; p = 0.80). The majority of cases were grade 2 in each of the groups (MSI-H 69.5% vs MSS 75.9%; p=0.63), and more aggressive grade 3 cases made up 17.0% in the MSI-H and 13.0% in the MSS cohort. As most cases were stage IA, only 25.4% had myometrial invasion equal to or greater than 50% in the MSI-H and 26.9% in the MSS cases. Lastly, there was a significant difference in lymphovascular space invasion (LVSI) between the two groups with more MSS cases having LVSI present (67.6%) than that seen in the MSI-H (39.0%) cases (p=0.02).

Table 5. Baseline patient characteristics by MSI-H and MSS status.

	MSI-H (N=59)	**MSS (N=108)**	**P value**
Mean Age (y)	63.0	59.5	0.84
Mean BMI (kg/m^2)	34.3	36.5	0.19
Histology, N (%)			0.60
Endometrioid	55 (93.2)	106 (98.2)	
Undifferentiated	1 (1.7)	1 (0.9)	
Mixed	3 (5.1)	1 (0.9)	
Stage, N (%)			0.80
IA	35 (59.3)	72 (66.7)	
IB	8 (13.6)	17 (15.7)	
II	3 (5.1)	5 (4.6)	
III/IV	8 (13.6)	14 (13.0)	
Unknown	5 (8.5)	--	
Grade, N (%)			0.63
1	6 (10.2)	12 (11.1)	
2	41 (69.5)	82 (75.9)	
3	10 (17.0)	14 (13.0)	
Unknown	2 (3.4)	--	
Depth of Myometrial Invasion, N (%)			0.46
No invasion	8 (13.6)	24 (22.2)	
< 50%	25 (42.4)	55 (50.9)	
≥ 50%	15 (25.4)	29 (26.9)	
Unknown	11 (18.6)	--	
LVSI, N (%)			**0.02***
Present	23 (39.0)	73 (67.6)	
Absent	24 (40.7)	33 (30.6)	
Unknown	12 (20.3)	2 (1.9)	

Abbreviations: BMI, body mass index; kg/m^2, kilograms per meter squared; LVSI, lymphovascular space invasion

IMMUNE MICROENVIRONMENT OF MSI-H ENDOMETRIAL CANCER COMPARED TO MSS TUMORS

The immune microenvironment in MSI-H versus MSS EC was examined using three fluorescent IHC multiplexing panels. The first panel evaluated positive staining of CD8 (CD8$^+$ T cells), granzyme B (activated CTLs or NK cells), CD68 (macrophages), PD-L1 (immune checkpoint ligand), and NKp46 (NK cells). Staining with the NKp46 antibody was difficult to optimize and ultimately resulted in nonspecific staining. As a result, this marker could not be analyzed. The second panel measured positive staining for CD3 (general T cell marker), CD4 (CD4$^+$ T cells), PD-L1 (immune checkpoint ligand), and CD11c (dendritic cell marker). Finally, the third panel evaluated positive staining of CD103 (intraepithelial T cell or dendritic cell marker) and CD8 (CD8$^+$ T cells). Representative images for each of the multiplexing panels are demonstrated in Figure 5. Markers repeated in multiple panels (PD-L1 and CD8) demonstrated substantial variation in overall total positive cell counts in subsequent multiplexing panels. However, as noted in Methods, batch effects for multiplex staining (due to differences in conditions between panels) make it necessary for comparison of these markers to only be performed within a multiplexing batch. PD-L1$^+$ staining showed a 1.2-1.4 fold difference in the stroma and a 1.4-2 fold difference in the tumor epithelial compartment. While CD8$^+$ staining had a 1.2-1.3 fold difference in the stroma and a 1.5-2.1 fold difference in the tumor epithelial compartment. Additionally, the counts in the tumor epithelial compartment may be less reliable due to the low overall positive cell counts which are reflected in the wider variation of fold difference within the tumor epithelial compartment.

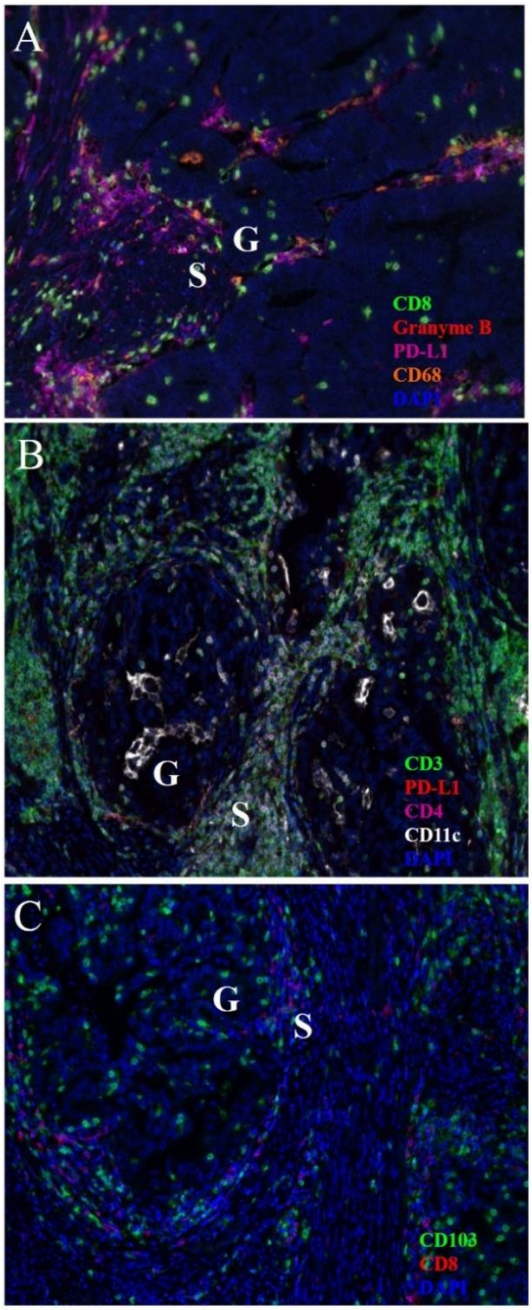

Figure 5. Fluorescent IHC multiplexing panel images.

(A) Representative image of IHC multiplexing panel 1 including: CD8 (green), Granzyme B (red), CD68 (orange), PD-L1 (magenta), and DAPI (blue). **(B)** Representative image of IHC multiplexing panel 2 including: CD3 (green), PD-L1 (red), CD4 (magenta), CD11c (white), and DAPI (blue). **(C)** Representative image of IHC multiplexing panel 3 including: CD 103 (green), CD8 (red), and DAPI (blue). S indicates peritumoral stroma; G indicates tumor glandular epithelium.

Details of the number of positively stained cells per marker within both the stromal and tumor epithelial compartments for the entire cohort are shown in Table 6 to enable comparison of the relative abundance of positive staining across different tissue compartments and markers (within each individual multiplex panel, as indicated on the table). Among all MSI-H tumors, the mean number of granzyme B^+, PD-$L1^+$, and $CD4^+$ staining cells were significantly higher within the tumor associated stroma. As other studies have looked at the percentage of PD-$L1^+$ cells, this was also assessed in our cohort to allow for comparison across studies. The percentage of PD-$L1^+$ staining stromal cells was also significantly increased in the MSI-H cases (59.2% vs 49.0%; $p<0.01$), but not in the tumor epithelium (5.4% vs 3.8%; $p=0.26$) when compared to MSS EC (Figure 6A and 6B). There was no statistically significant difference seen in the mean number of stromal cells staining positive for CD3, CD8, CD103, CD68, or CD11c between MSI-H and MSS tumors.

In evaluating the tumor epithelial compartment, the mean number of granzyme B^+ staining cells in the MSI-H group was significantly higher, while the mean number of $CD68^+$ staining cells within the tumor epithelial compartment was significantly lower in the MSI-H versus MSS cases. There was no significant difference seen in mean number of cells staining positive for CD3, CD4, CD8, CD103, CD11c, or PD-L1 between MSI-H and MSS tumors in the tumor epithelial compartment.

Table 6. Comparison of positive staining cell counts between MSI-H and MSS ECs

Marker	**All MSI-H EC** Mean No of positive cells/mm^2 (range)	**MSS EC** Mean No of positive cells/mm^2 (range)	**P value**
Stromal Compartment			

CD8[1]	50.7 (0-180.1)	39.4 (0-342.6)	0.06
Granzyme B[1]	114.9 (0.1-440.4)	75.8 (0-657.2)	**<0.01***
CD68[1]	29.1 (0-156.6)	22.9 (0-127.9)	0.86
PD-L1[1]	291.6 (107.6-434.2)	240.5 (28.6-408.3)	**<0.01***
CD3[2]	89.5 (0.3-282.2)	69.7 (3.4-179.0)	0.05
CD4[2]	25.4 (0-82.4)	17.8 (0.2-76.1)	**0.02***
CD11c[2]	22.1 (0-133.9)	17.4 (0-133.3)	0.49
CD103[3]	7.9 (0-107.4)	4.8 (0-128.8)	0.30
Tumor Epithelial Compartment			
CD8[1]	7.9 (0-53.5)	5.1 (0-38.4)	0.07
Granzyme B[1]	38.9 (0-391.0)	32.6 (0-433.8)	**<0.01***
CD68[1]	1.8 (0-8.5)	2.8 (0-19.2)	**0.03***
PD-L1[1]	21.3 (0-243.8)	15.4 (0-214.2)	0.29
CD3[2]	51.5 (0.1-349.6)	37.9 (1.0-236.1)	0.23
CD4[2]	25.6 (0-255.8)	17.1 (0-130.4)	0.31
CD11c[2]	8.9 (0-83.1)	11.1 (0-87.7)	0.27
CD103[3]	23.5 (0-111.6)	17.7 (0-92.5)	0.48

[1]Multiplex panel 1; [2]Multiplex panel 2; [3]Multiplex panel 3; *p<0.05. Abbreviations: MSI-H, high microsatellite instability; MSS, microsatellite stable; EC endometrial cancer.

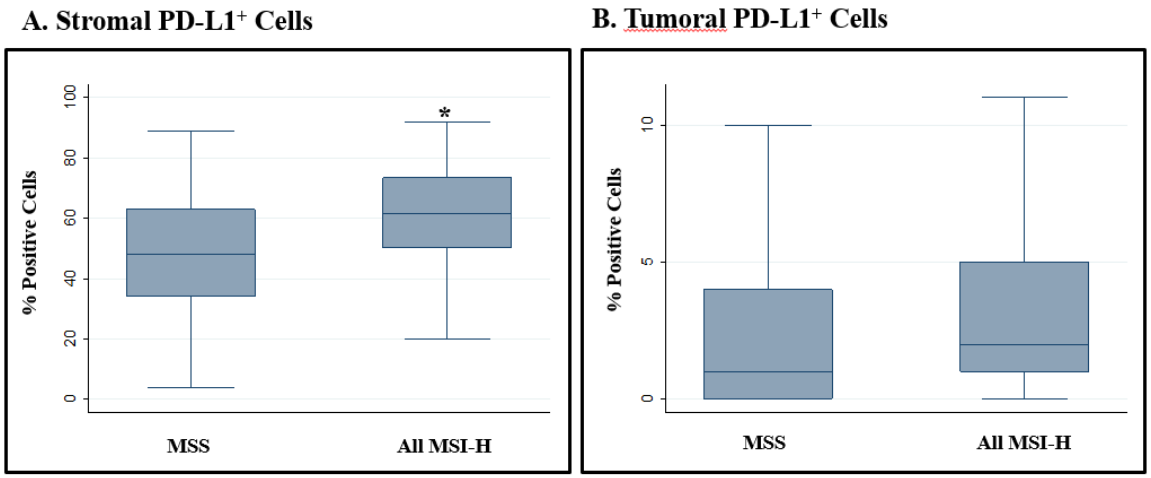

Figure 6. MSI-H ECs show increased stromal PD-L1 expression compared to MSS ECs.

(A) Box plot representing the percentage of PD-L1$^+$ cells within the peritumoral stroma compartment of MSI-H vs MSS EC. **(B)** Box plot of the percentage of PD-L1$^+$ cells

within the tumor intraepithelial compartment of MSI-H vs MSS EC. The center line of the box plot indicates the median. *p value <0.05. Abbreviations: MSI-H, high microsatellite instability; MSS, microsatellite stable.

Comparison of marker colocalization in each tissue compartment is shown in Table 7. Co-staining of $CD8^+$ and granzyme B^+ cells was analyzed to assess the number of activated CTLs within the two groups. In all MSI-H tumors, there were significantly more activated CTLs in both the stromal and in the tumor epithelial compartments. There was also a significant increase seen in colocalization of PD-$L1^+$ and $CD11c^+$ staining cells (PD-$L1^+$ dendritic cells) among the stroma in all MSI-H versus MSS EC, but not in the tumor epithelial compartment. Stromal colocalization staining for activated CTLs and PD-$L1^+$ dendritic cells is shown in Figures 7A and 7C. Colocalization of $CD3^+$ and $CD4^+$ staining cells, denoting T helper cells, demonstrated a significant increase in mean number of cells between all MSI-H and MSS in the stroma, but not within the tumor epithelial compartment. Lastly, no difference was seen in colocalization of $CD103^+$ and $CD8^+$ positive cells (intraepithelial $CD8^+$ cells) or of PD-$L1^+$ and $CD68^+$ staining cells (PD-$L1^+$ macrophages) in either of the compartments in all MSI-H versus MSS EC. Stromal PD-$L1^+$ macrophages are represented in Figure 7B.

Table 7. Comparison of co-staining positive cell counts between MSI-H and MSS ECs

Marker	**All MSI-H EC** Mean No of positive cells/mm^2 (range)	**All MSS EC** Mean No of positive cells/mm^2 (range)	**P value**
Colocalization in Stromal Compartment			
$CD8^1$/Granzyme B^1	45.6 (0.7-179.1)	28.0 (0-228.4)	**<0.01***
PD-$L1^1$/$CD68^1$	25.1 (0-148.4)	15.6 (0-93.8)	0.49

CD3[2]/CD4[2]	24.9 (0-82.3)	17.4 (0.2-75.7)	**0.02***
PD-L1[2]/CD11c[2]	6.7 (0-66.3)	4.3 (0-97.9)	**0.01***
CD8[3]/CD103[3]	5.22 (0-83.0)	2.92 (0-94.0)	0.26
Colocalization in Tumor Epithelial Compartment			
CD8[1]/Granzyme B[1]	5.7 (0-53.5)	2.3 (0-11.6)	**0.03***
PD-L1[1]/CD68[1]	0.5 (0-5.5)	0.2 (0-1.8)	0.74
CD3[2]/CD4[2]	25.0 (0-255.8)	16.8 (0-130.3)	0.25
PD-L1[2]/CD11c[2]	0.4 (0-11.3)	0.2 (0-1.6)	0.14
CD8[3]/CD103[3]	1.7 (0-43.3)	0.51 (0-1.5)	0.20

[1]Multiplex panel 1; [2]Multiplex panel 2; [3]Multiplex panel 3; *p<0.05. Abbreviations: MSI-H, high microsatellite instability; MSS, microsatellite stable; EC, endometrial cancer.

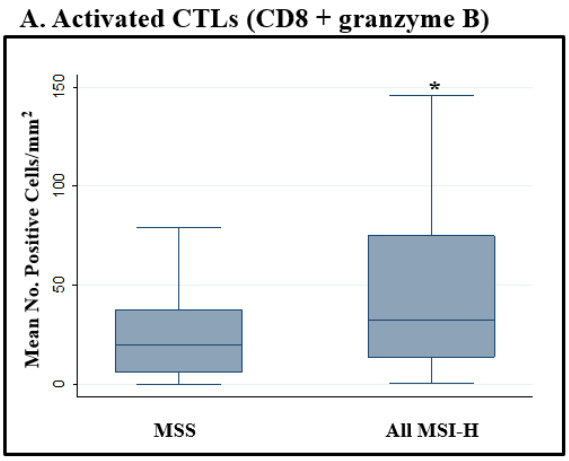

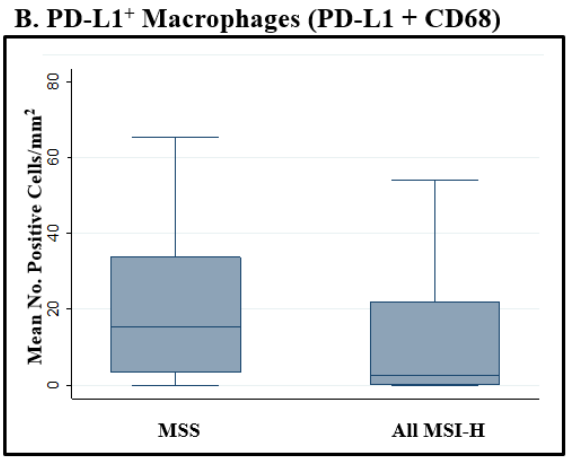

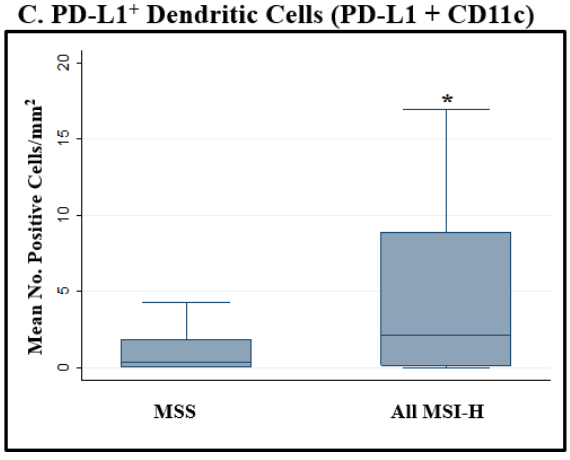

Figure 7. MSI-H ECs have increased stromal activated CTLs and PD-L1$^+$ dendritic cells compared to MSS ECs.

(A) Box plots demonstrating the number of positive cells per mm^2 of activated CTLs (co-staining of CD8 and granzyme B), **(B)** PD-L1$^+$ macrophages (co-staining of PD-L1 and CD68), and **(C)** PD-L1$^+$ dendritic cells (co-staining of CD11c and PD-L1) in the peritumoral stroma. The center box plot line indicates the median positive cell count. *p value <0.05. Abbreviations: CTL, cytotoxic T lymphocyte; MSS, microsatellite stable; MSI-H, high microsatellite instability.

SPORADIC MSI-H ENDOMETRIAL CANCER

A secondary sub-analysis was then performed to assess differences in the immune microenvironment of sporadic MSI-H EC compared to MSS tumors (excluding LS MSI-H cases). This analysis included only MSI-H tumors with MLH1 promoter methylation compared to matched MSS tumors. The overall mean values for each marker are depicted in Table 8. Within this subgroup, the number of granzyme B$^+$, CD3$^+$, and CD4$^+$ staining cells within both the tumor associated stroma and the tumor epithelial compartments was higher among the sporadic MSI-H versus MSS cases. This was in comparison to only increased stromal and tumor epithelial granzyme B$^+$ staining cells and stromal CD4$^+$ staining cells in all MSI-H versus MSS cases. The percentage of PD-L1$^+$ staining cells (61.1% vs 45.3%; p<0.01) was significantly higher in the stromal compartment for sporadic MSI-H versus MSS cases like that seen in all MSI-H cases (Fig 8A), as well as within the tumor epithelial compartment (sporadic MSI-H 6.3% vs MSS 2.3%; p=0.03) (Fig 8B). As seen in all MSI-H versus MSS cases, there was no difference in the mean number of positive staining cells within the stroma for CD8, CD68, CD11c, or CD103 in sporadic MSI-H compared to MSS EC. In the tumor epithelial compartment, mean positive staining cell counts for CD8, CD68, CD11c, or CD103 were also not significantly different between sporadic MSI-H versus MSS cases.

Table 8. Comparison of positive staining cell counts between sporadic MSI-H and MSS ECs.

Marker	**Sporadic MSI-H EC** Mean No of positive cells/mm^2 (range)	**MSS EC** Mean No of positive cells/mm^2 (range)	**P value**
Stromal Compartment			
CD8[1]	36.9 (0-133.7)	45.3 (0-342.6)	0.62
GranzymeB[1]	107.4 (12.3-377.9)	84.1 (0-657.2)	**0.02***
CD68[1]	36.6 (0.5-156.6)	20.9 (0-127.9)	0.25
PD-L1[1]	297.3 (112.7-433.9)	225.9 (28.6-408.3)	**<0.01***
CD3[2]	88.1 (11.7-233.7)	65.9 (3.4-179.0)	**0.03***
CD4[2]	26.6 (2.7-73.4)	16.5 (0.2-76.1)	**<0.01***
CD11c[2]	22.8 (0-133.9)	16.5 (0-133.3)	0.21
CD103[3]	7.2 (0-107.4)	5.7 (0-128.8)	0.40
Tumor Epithelial Compartment			
CD8[1]	5.9 (0.1-20.1)	5.5 (0-38.4)	0.30
Granzyme B[1]	43.5 (0-391.0)	35.2 (0-433.8)	**<0.01***
CD68[1]	2.4 (0-8.5)	2.8 (0-19.2)	1.0
PD-L1[1]	25.0 (0.2-243.8)	10.0 (0-68.3)	**0.02***
CD3[2]	56.5 (4.0-349.6)	33.3 (1.4-181.7)	**0.04***
CD4[2]	29.7 (0.9-255.8)	14.5 (0.1-117.4)	**0.04***
CD11c[2]	9.9 (0-83.1)	11.6 (0-87.7)	0.63
CD103[3]	24.8 (0-111.6)	18.4 (0-92.5)	0.43

[1]Multiplex panel 1; [2]Multiplex panel 2; [3]Multiplex panel 3; *p<0.05. Abbreviations: MSI-H, high microsatellite instability; MSS, microsatellite stable; EC, endometrial cancer.

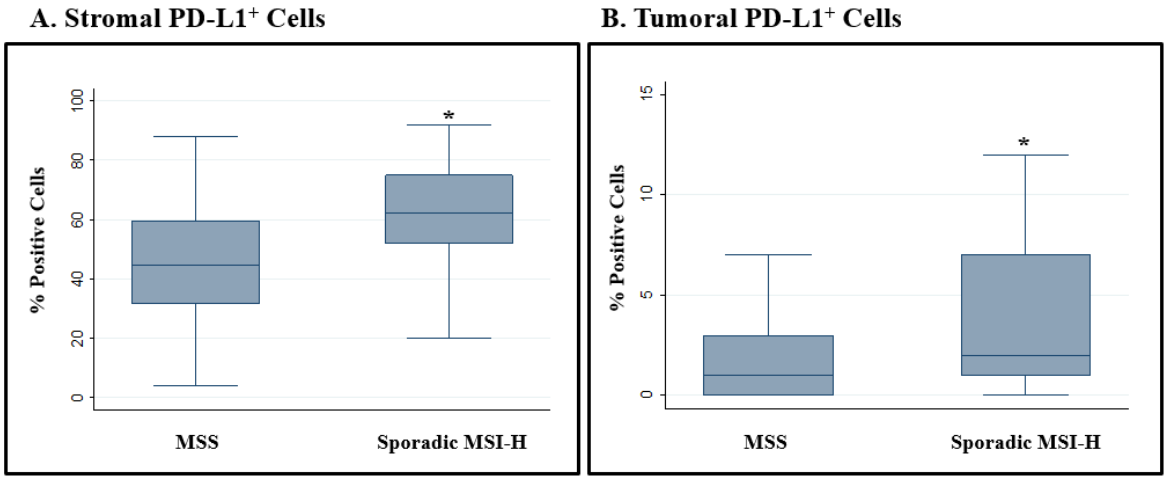

Figure 8. Sporadic MSI-H ECs show increased stromal and tumor epithelial PD-L1 expression compared to MSS ECs.

(A) Box plot representing the percentage of PD-L1$^+$ cells within the peritumoral stroma compartment of sporadic MSI-H vs MSS EC. **(B)** Box plot of the percentage of PD-L1$^+$ cells within the tumor intraepithelial compartment of sporadic MSI-H vs MSS EC. The center line of each box plot represents the median. *p value <0.05. Abbreviations: MSI-H, high microsatellite instability; MSS, microsatellite stable.

Table 9 compares positive co-staining cell counts within the stromal and tumor epithelial compartments. Sporadic MSI-H cases demonstrated an increase in stromal PD-L1$^+$ dendritic cells (co-staining of PD-L1 and CD11c). This finding was similar to that seen in the analysis of all MSI-H versus MSS cases. There was no difference in PD-L1$^+$dendritic cells in the tumor epithelial compartment of sporadic MSI-H compared to MSS cases. There was also an increase in PD-L1$^+$ macrophages (co-staining PD-L1 and CD68) in the stroma of sporadic MSI-H versus MSS cases which was not seen in the

analysis of all MSI-H versus MSS cases, but no differences in the intraepithelial compartment. Additionally, T helper cells (co-staining of CD3 and CD4) were significantly increased in both the stromal and tumor epithelial compartments in sporadic MSI-H versus MSS cases in contrast to only in the stroma of all MSI-H versus MSS cases. No difference was seen in activated CTLs (co-staining of CD8 and granzyme B) in either the stroma or tumor epithelial compartment in contrast to that seen in all MSI-H compared to MSS EC. There was also no difference seen in intraepithelial $CD8^+$ cells (co-staining of CD103 and CD8) in either the stromal or tumor epithelial compartments like that in all MSI-H versus MSS EC. Box plot comparisons of stromal CTLs, PD-$L1^+$ macrophages, and PD-$L1^+$ dendritic cells are shown in Figures 9A, 9B, and 9C.

Table 9. Comparison of co-staining positive cell counts between sporadic MSI-H and MSS ECs.

Marker	**Sporadic MSI-H EC** Mean No of positive cells/mm^2 (range)	**MSS EC** Mean No of positive cells/mm^2 (range)	**P value**
Colocalization in the Stromal Compartment			
CD8[1]/Granzyme B[1]	32.4 (0.7-98.3)	31.0 (0-228.4)	0.41
PD-L1[1]/CD68[1]	31.3 (0-148.4)	13.4 (0-93.8)	**0.04***
CD3[2]/CD4[2]	26.0 (2.4-73.1)	16.0 (0.2-75.7)	**0.01***
PD-L1[2]/CD11c[2]	6.5 (0-66.3)	3.7 (0-97.9)	**0.01***
CD8[3]/CD103[3]	4.3 (0-72.1)	3.4 (0-13.3)	0.36
Colocalization in the Tumor Epithelial Compartment			
CD8[1]/Granzyme B[1]	3.8 (0-18.4)	2.5 (0-11.6)	0.15
PD-L1[1]/CD68[1]	0.7 (0-5.5)	0.2 (0-1.8)	0.05
CD3[2]/CD4[2]	29.1 (0.9-255.8)	14.1 (0.1-117.2)	**0.03***
PD-L1[2]/CD11c[2]	0.2 (0-1.1)	0.2 (0-1.6)	0.34
CD8[3]/CD103[3]	0.8 (0-8.3)	0.5 (0-13.3)	0.30

[1]Multiplex panel 1; [2]Multiplex panel 2; [3]Multiplex panel 3; *$p<0.05$. Abbreviations: MSI-H, high microsatellite instability; MSS, microsatellite stable: EC, endometrial cancer.

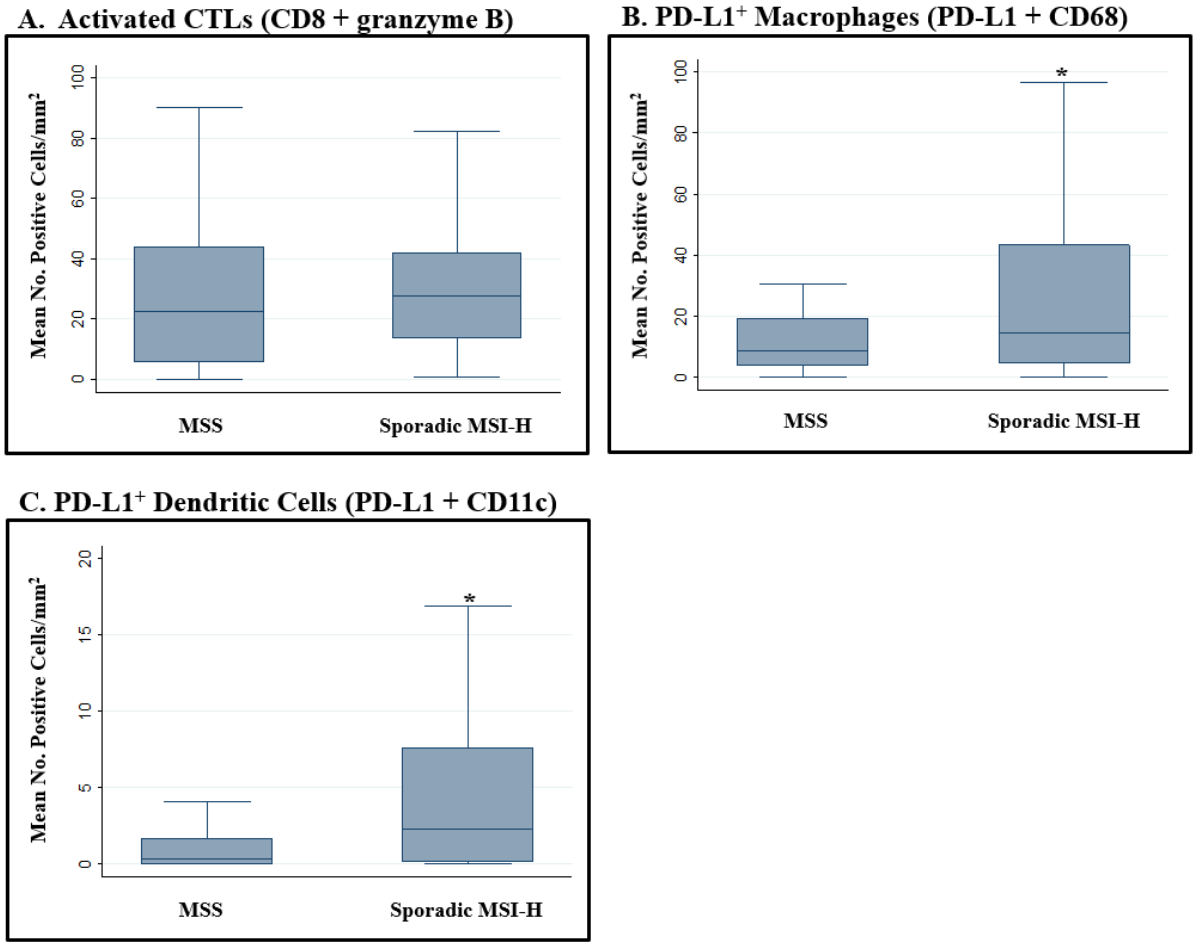

Figure 9. Sporadic MSI-H ECs have increased stromal PD-L1$^+$ macrophages and PD-L1$^+$ dendritic cells compared to MSS ECs.

(A) Box plots demonstrating the number of positive cells per mm^2 of activated CTLs (co-staining of CD8 and granzyme B), **(B)** PD-L1$^+$ macrophages (co-staining of PD-L1 and CD68), and **(C)** PD-L1$^+$ dendritic cells (co-staining of CD11c and PD-L1) in the peritumoral stroma. The center box plot line indicates the median positive cell count. *p value <0.05. Abbreviations: CTL, cytotoxic T lymphocyte; MSS, microsatellite stable; MSI-H, high microsatellite instability.

LYNCH-RELATED MSI-H ENDOMETRIAL CANCER

Lastly, evaluation of the differences in the immune microenvironment in LS MSI-H EC compared to matched MSS cases was conducted, and mean positive staining cell

counts are depicted below in Table 10. LS MSI-H EC demonstrated a significantly higher mean number of granzyme B^+ staining cells within the tumor associated stroma compared to MSS tumors as was also seen in all MSI-H and sporadic MSI-H analyses. In contrast to that seen in the all MSI-H and sporadic MSI-H versus MSS analyses, there were also a significantly higher mean number of $CD8^+$ staining cells in both the stromal and tumor epithelial compartments among LS MSI-H versus MSS tumors. The mean number of $CD68^+$ staining cells was found to be significantly reduced in both the stromal and tumor epithelial compartments in LS MSI-H cases compared to MSS EC, in contrast to all MSI-H versus MSS analyses where $CD68^+$ positive staining cells were only reduced in the tumor epithelial compartment.

There was no significant difference observed in the mean number of granzyme B^+ staining cells within the tumor epithelial compartment between LS MSI-H and MSS EC in contrast to the other analyses. Mean positive staining cell counts in the stroma between LS MSI-H and MSS tumors showed no difference in CD3, CD4, CD103, or CD11c as compared to the increased $CD3^+$ and $CD4^+$ staining cell counts in sporadic MSI-H versus MSS EC. In the tumor epithelial compartment, mean positive staining cells counts were not significantly different between LS MSI-H and MSS EC for CD3, CD4, CD11c, or CD103. This finding was similar to that seen in the analyses of all MSI-H compared to matched MSS EC. There was no difference in mean PD-$L1^+$ staining cells between the LS MSI-H and MSS EC in either the stromal or tumor epithelial compartments which was different from the increased PD-$L1^+$ staining among stromal cells in both sporadic MSI-H and all MSI-H versus MSS analyses. There was also no difference in mean percentage of PD-$L1^+$ staining cells in the stroma (LS MSI-H 56.2% vs MSS 58.1%; p=0.92) and tumor

epithelial (LS MSI-H 3.5% vs MSS 7.2%; p=0.15) compartments in LS MSI-H versus MSS EC (Figure 10A and 10B).

Table 10. Comparison of positive staining cell counts between LS MSI-H and MSS ECs.

Marker	**LS MSI-H EC** Mean No of positive cells/mm^2 (range)	**MSS EC** Mean No of positive cells/mm^2 (range)	**P value**
Stromal Compartment			
CD8[1]	78.4 (6.6-180.1)	25.9 (0-86.4)	**<0.01***
Granzyme B[1]	150.7 (12.1-440.4)	58.3 (2.3-323.9)	**0.01***
CD68[1]	14.6 (0-58.0)	28.3 (0-82.7)	**0.03***
PD-L1[1]	281.5 (107.6-434.2)	274.0 (118.6-387.6)	0.54
CD3[2]	94.0 (0.3-282.2)	80.9 (17.2-167.4)	0.82
CD4[2]	21.7 (0-82.4)	21.8 (0.7-63.1)	1.0
CD11c[2]	19.6 (0-92.1)	20.1 (0-75.5)	0.46
CD103[3]	9.44 (0-85.1)	2.61 (0-34.3)	0.81
Tumor Epithelial Compartment			
CD8[1]	12.0 (0.6-53.5)	4.1 (0.1-14.0)	**0.04***
Granzyme B[1]	46.6 (0.6-248.8)	28.3 (0.1-402.6)	0.10
CD68[1]	0.7 (0-5.7)	3.1 (0.2-11.8)	**<0.01***
PD-L1[1]	15.6 (0-71.4)	29.2 (0.2-214.2)	0.15
CD3[2]	36.0 (0.1-120.0)	51.3 (1.0-236.1)	0.42
CD4[2]	12.6 (0-92.1)	24.9 (0-130.4)	0.23
CD11c[2]	5.9 (0-24.7)	9.8 (0-39.0)	0.12
CD103[3]	19.1 (0-73.9)	16.5 (0-50.8)	0.79

[1]Multiplex panel 1; [2]Multiplex panel 2; [3]Multiplex panel 3; *p<0.05. Abbreviations: LS MSI-H, Lynch syndrome high microsatellite instability; MSS, microsatellite stable; EC endometrial cancer.

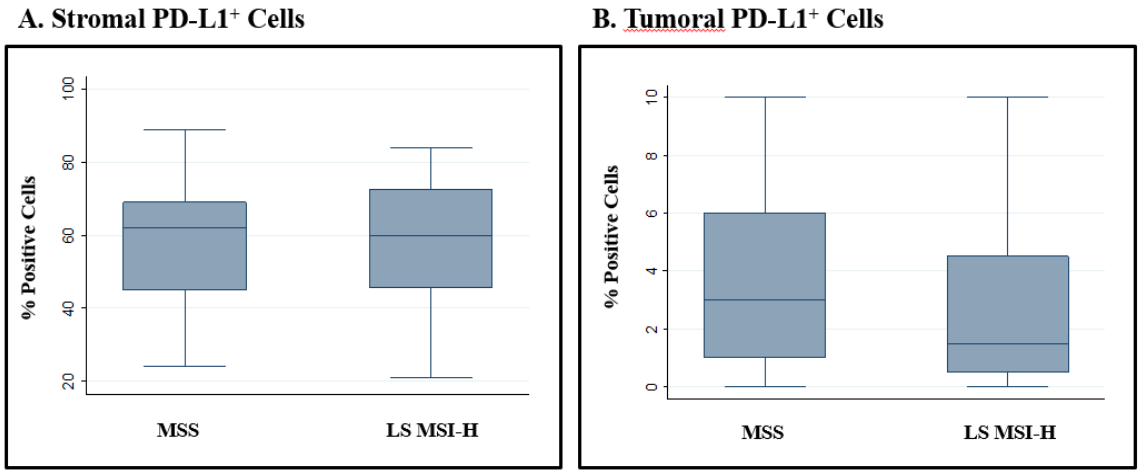

Figure 10. LS MSI-H ECs show no difference in stromal or tumoral PD-L1 expression compared to MSS ECs.

(A) Box plot representing the percentage of PD-L1$^+$ cells within the peritumoral stroma compartment of LS MSI-H vs MSS EC. **(B)** Box plot of the percentage of PD-L1$^+$ cells within the tumor intraepithelial compartment of LS MSI-H vs MSS EC. The center line of each box plot represents the median. Abbreviations: LS MSI-H, Lynch syndrome high microsatellite instability; MSS, microsatellite stable.

Colocalization staining is represented in Table 11. There was a significantly higher mean number of activated CTLs (co-staining with CD8 and granzyme B) in LS MSI-H versus MSS cases with higher stromal and tumor epithelial positive cells as was seen in all MSI-H compared to matched MSS EC. Within the tumoral epithelial compartment, there was a significant decrease in colocalization of PD-L1 and CD68 (PD-L1$^+$ macrophages) in LS MSI-H compared to MSS EC, but no difference within the stroma. Lastly, there was no difference seen in colocalization of PD-L1 and CD11c (PD-L1$^+$ dendritic cells), CD3 and CD4 (T helper cells), or CD103 and CD8 (CD8$^+$ intraepithelial cells) in either of the compartments between LS MSI-H and MSS EC. This was in contrast to the increased stromal PD-L1$^+$ dendritic cells seen in the comparison of all MSI-H and sporadic MSI-H cases to matched MSS

Table 11. Comparison of co-staining positive cell counts between LS MSI-H and MSS ECs.

Marker	LS MSI-H EC Mean No of positive cells/mm^2 (range)	MSS EC Mean No of positive cells/mm^2 (range)	P value
Colocalization in the Stromal Compartment			
CD8[1]/Granzyme B[1]	68.4 (6.1-179.1)	21.4 (0.2-74.4)	**0.01***
PD-L1[1]/CD68[1]	4.1 (0-15.0)	7.5 (0-21.0)	0.06
CD3[2]/CD4[2]	21.7 (0-82.3)	21.5 (0.7-61.8)	0.98
PD-L1[2]/CD11c[2]	7.4 (0-26.8)	6.2 (0-48.9)	0.56
CD8[3]/CD103[3]	7.45 (0-83.0)	1.68 (0-33.7)	0.73
Colocalization in the Tumor Epithelial Compartment			
CD8[1]/Granzyme B[1]	9.1 (0.3-53.5)	2.0 (0-6.9)	**0.03***
PD-L1[1]/CD68[1]	0.8 (0-5.0)	2.5 (0-12.0)	**0.02***
CD3[2]/CD4[2]	12.5 (0-47.5)	24.8 (0-130.3)	0.22
PD-L1[2]/CD11c[2]	1.2 (0-11.3)	0.1 (0-0.6)	0.23
CD8[3]/CD103[3]	4.0 (0-43.3)	0.6 (0-11.2)	0.58

[1]Multiplex panel 1; [2]Multiplex panel 2; [3]Multiplex panel 3; *$p<0.05$. Abbreviations: LS MSI-H, Lynch syndrome high microsatellite instability; MSS, microsatellite stable; EC, endometrial cancer.

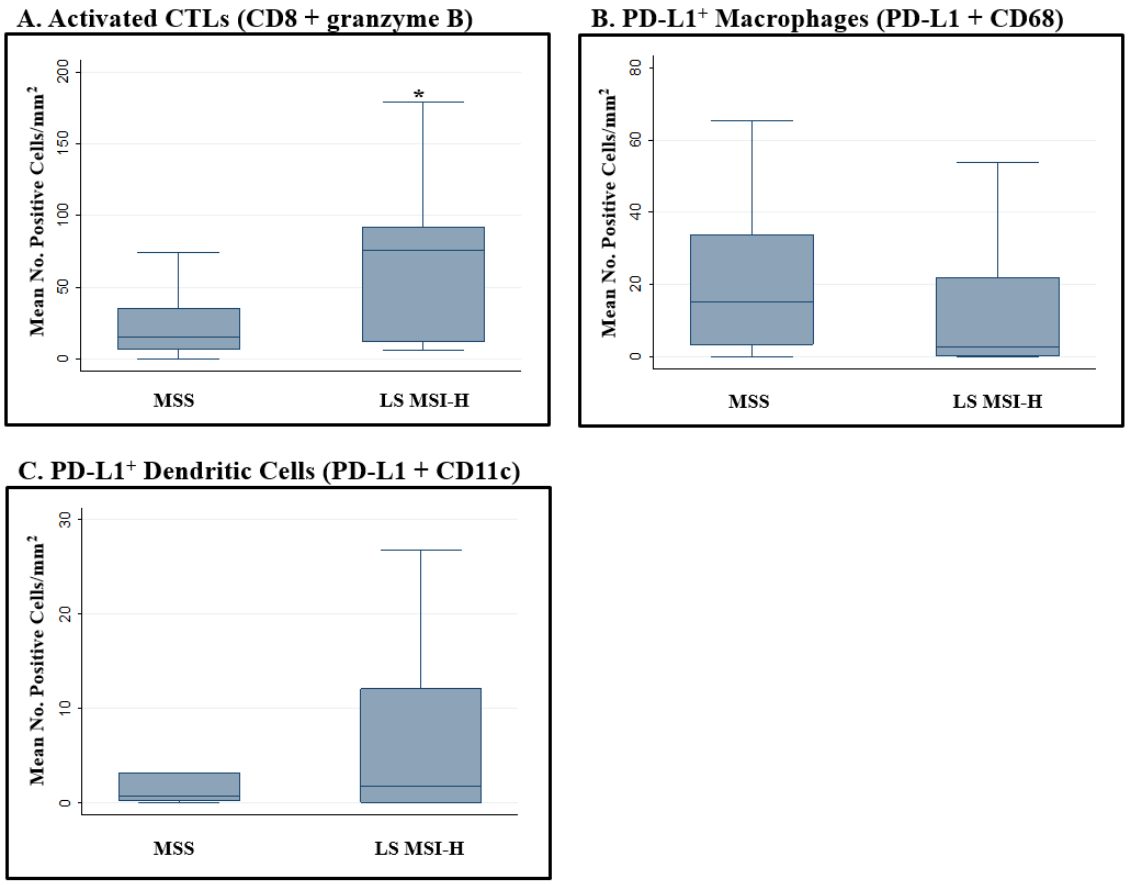

Figure 11. LS MSI-H ECs have increased activated CTLs compared to MSS ECs.

(A) Box plots demonstrating the number of positive cells per mm^2 of activated CTLs (co-staining of CD8 and granzyme B), **(B)** PD-$L1^+$ macrophages (co-staining of PD-L1 and CD68), and **(C)** PD-$L1^+$ dendritic cells (co-staining of CD11c and PD-L1) in the peritumoral stroma. The center box plot line indicates the median positive cell count. *p value <0.05. Abbreviations: CTL, cytotoxic T lymphocyte; MSS, microsatellite stable; LS MSI-H, Lynch syndrome high microsatellite instability.

Chapter 4: Discussion

As our understanding of the molecular and clinical heterogeneity of EC has grown, it is clear that a variety of therapeutic approaches will be required for successful outcomes both as upfront treatment and for recurrent/advanced cases. While clinical trials of molecularly targeted single agents have shown disappointing results in EC, immunotherapy has emerged as a promising therapeutic option in multiple tumor types that previously had limited treatment options and poor overall prognosis (65, 66). This immunologic tumor-directed response is thought to be activated by tumor-specific neoantigens that correlate with somatic mutational load and infiltration of $CD8^+$ CTLs. This thesis sought to provide a detailed analysis of the immune microenvironment of MSI-H EC and potential implications for response to immunotherapy. Previous studies of the immune microenvironment in EC were limited and had not fully investigated sporadic MSI-H and LS MSI-H cases (56, 59). These studies are critical to identifying therapeutic targets for advanced and recurrent EC given the limited treatment options should patients fail standard chemotherapy. Currently, there are no targeted therapies in clinical use for molecular subsets of EC, but early studies of the immune microenvironment of MSI-H EC have suggested that these tumors may be more immunogenic and thus responsive to immunotherapy (56, 59).

Analysis of TCGA uterine data suggested increased CTL activity in MSI-H compared to MSS EC. This was shown through increased activation of the granzyme B pathway in MSI-H EC overall which leads to targeted cell apoptosis through CTL directed cytolytic activity. Additionally, the more specific immune-related TCGA analysis identified upregulated mRNA levels of several T cell effector genes (*CD8a*, *MICB*,

CXCL9, and *ICOS*), that further supports at least an initial enhanced anti-tumoral response in MSI-H versus MSS EC.

The comprehensive examination of the immune cell populations in MSI-H and MSS EC identified differences in the immune microenvironment of these two subtypes. MSI-H tumors had increased granzyme B^+ staining cells and CTL activation within both the tumor epithelium and tumor associated stroma and increased Helper T cells in the stroma. This suggests an immune mediated anti-tumor response in this subset of ECs. Stromal PD-L1 expression was also significantly increased in MSI-H EC and reflects immune response exhaustion and suppression. Among all MSI-H cases, however, there was no significant difference in other T cell populations ($CD3^+$, $CD8^+$, and $CD103^+$ intraepithelial T cells), $CD68^+$ macrophages or $CD11c^+$ dendritic cells when compared to MSS tumors.

Sub-analysis of sporadic MSI-H EC also demonstrated a difference in the immune microenvironment compared to MSS tumors. Sporadic MSI-H EC had increased $CD3^+$, $CD4^+$, and granzyme B^+ cells in the stroma and tumor epithelium compared to MSS tumors reflecting an immune related response in these tumors. Additionally, increased stromal and tumoral PD-L1 expression along with increased stromal PD-$L1^+$ macrophages and PD-$L1^+$ dendritic cells was seen compared to MSS EC.

Lastly, sub-analysis of LS MSI-H showed increased CTL activation compared to MSS EC. This was demonstrated by increased stromal $CD8^+$ cells, granzyme B^+ cells, and activated CTLs in LS MI-H versus MSS EC. $CD8^+$ cells and activated CTLs were also increased in the tumor epithelial compartment in LS MSI-H versus MSS EC. In contrast to the all MSI-H and sporadic MSI-H versus MSS analyses, LS MSI-H cases demonstrated

no difference in PD-L1$^+$ staining in the stromal or tumor epithelial compartment compared to MSS EC. Additionally, CD68$^+$ cells were significantly reduced in the stromal and tumor epithelial compartments of LS MSI-H versus MSS tumors.

Analysis of both immune cell markers and markers of immune response activity is needed to provide a complete view of the immune microenvironment. Previously, studies in MSI-H and POLE ECs have found elevated levels of CD3$^+$ and CD8$^+$ infiltrating lymphocytes suggesting increased tumor immunogenicity in these subtypes (56, 59). Additionally, other studies have shown that CD103 expression enhances retention of T cells in the tumor epithelium and is also associated with polarization of cytolytic granules (47, 67). This then primes the T cell for cytotoxic activity once antigen recognition has occurred. Although our study did not show a difference in CD8$^+$ or CD103$^+$ cells between all MSI-H and MSS EC, there was a significant difference in granzyme B$^+$ cells and activated CTLs as demonstrated by colocalization of CD8 and granzyme B. This provides further evidence of a more active immune microenvironment in MSI-H EC, and suggests that the CTLs that are present are activated and capable of mounting an anti-tumor immune response. Inevitability, however, such activation is followed by exhaustion and inhibition via immune checkpoint expression, such as PD-L1.

While an overall characterization of immune cell types is informative, an understanding of expression patterns for specific markers is also important for improved immunotherapy studies and clinical trials. PD-L1 expression on tumor versus stromal cells may have important implications for therapeutic response to anti-PD-L1 therapies, but expression varies among tumor types (41, 42). Our study found low overall expression of tumoral PD-L1$^+$ cells and no difference in expression between all MSI-H and MSS EC.

However, we did find elevated levels of stromal cell PD-L1 expression with a significant increase in both all MSI-H and sporadic MSI-H versus matched MSS EC. Additionally, sporadic MSI-H also showed increased tumoral PD-L1 expression versus MSS EC. Although many studies have focused on tumor PD-L1 expression and its ability to predict response to anti-PD-1 and anti-PD-L1 therapy, its role as a biomarker remains unclear (41, 42). Further evaluation of PD-L1 expression among tumor types prior to treatment is needed, as well as, in responders and non-responders following immune checkpoint blockade therapy.

To further define the stromal PD-L1 expressing cells in our study, colocalization analysis of PD-L1 with both CD68 (macrophages) and CD11c (dendritic cells) was conducted. Overall there was no difference between all MSI-H and MSS EC in the number of CD68 or CD11c cells positive alone, but there was an increase in those co-expressing PD-L1 and CD11c (PD-L1$^+$ dendritic cells). The sporadic MSI-H sub-analysis also showed an elevated number of PD-L1$^+$ macrophages and PD-L1$^+$ dendritic cells compared to MSS EC, suggesting that both macrophages and dendritic cells may be key regulators of immune inhibition in the sporadic MSI-H EC microenvironment. This finding along with the correlation of PD-L1 expression on CD163 myeloid cells in MSI-H colorectal cancers, seen in other studies, suggests an alternate mechanism for immune response inhibition in these tumors from direct tumor cell suppression. Other immune checkpoints are also likely contributing to immune suppression, as suggested by increased *LAG-3* gene mRNA levels in MSI-H tumors from our TCGA analysis. As therapies targeting these other immune cell populations and immune checkpoints (i.e. TAMs and LAG-3) are becoming

available, additional studies are needed to further characterize these populations in MSI-H EC in order to expand treatment options.

Looking more closely at the sub-analysis of sporadic MSI-H EC, sporadic MSI-H tumors demonstrate both increased markers of immune cell infiltration and immune suppression compared to MSS EC. MSI-H EC had increased $CD3^+$, $CD4^+$, and $PD\text{-}L1^+$ staining cell populations in both the stromal and tumor epithelial compartments compared to matched MSS tumors. From these findings we can conclude that sporadic MSI-H, compared to MSS ECs, have increased immune cell infiltration and subsequent suppression of the immune response through checkpoint activation. These findings most closely mirror those found in the other MSI-H EC and colorectal microenvironment studies previously discussed, and suggest that sporadic MSI-H EC would respond favorably to single agent immune checkpoint blockade.

The role of immune checkpoint expression in LS MSI-H ECs, on the other hand, is less clear. Sub-analysis of LS MSI-H EC demonstrated increased $CD8^+$ and active CTLs in both the stroma and tumor epithelial compartments, but no difference in PD-L1 expression when compared to matched MSS cases. Similar to sporadic MSI-H versus MSS EC analysis, LS MSI-H EC also appears to promote an immunogenic microenvironment, but the same PD-L1 checkpoint expression was not seen. We can speculate that other immune checkpoints such as CTLA-4, TIM-3 (T cell immunoglobulin and mucin-domain containing-3) or LAG-3 may play a larger role in this subtype. Further studies specifically evaluating the expression of CTLA-4, TIM-3, LAG-3, and other immune checkpoints markers are needed to more clearly define immune checkpoint activity in these tumors, and to draw a more complete picture of the LS MSI-H immune microenvironment in EC.

Additionally, in some instances single agent immune checkpoint blockade is insufficient to overcome immune inhibition while combination therapy is able to target multiple immune checkpoint pathways (65, 68). In melanoma, combination anti-CTLA-4 and anti-PD-1 therapy has shown particular benefit in patients with PD-L1 negative tumors (65). Additionally, synergistic effects of combination immune checkpoint blocking agents have been shown in preclinical trials of combination anti-TIM-3 or anti-LAG-3 with anti-PD-1. Such combination therapies may provide more clinical benefit in LS MSI-H EC than single agent immune checkpoint blockade (69, 70). Along with this, consideration of combination immunotherapy and traditional cytotoxic agents may further improve response rates. In non-small cell lung cancer, preliminary phase I studies have shown activity and tolerability of combination of immune checkpoint blockade and chemotherapeutic agents (71, 72). This may be of particular importance in LS MSI-H EC where there is suggestion that the immune checkpoint expression is less robust. Here alternative immune checkpoint blockade or combination therapies are likely required.

Overall, this study provides new insight into the immune microenvironment related to MSI status in EC. It is the largest cohort assessing the immune microenvironment of MSI-H EC and the first to specifically investigate LS MSI-H EC cases. This large cohort was also matched to reduce confounding factors that influence immune cell populations and immune marker status (matched according to histology, grade, stage, age at diagnosis and BMI). There may, however, be some decrease in the overall differences of positive cell counts seen between MSI-H and MSS EC as MSS EC cases had higher rates of LVSI which is a known risk factor for disease recurrence. In addition to this unique sample set,

immune microenvironment characterization was more powerful due to the use of multiplexed IHC coupled with digital imaging for quantitation and colocalization analysis.

This study overcomes limitations observed in previous immune cell studies in EC, such as evaluation of limited high powered fields and inconsistent quantitation and scoring strategies. Vectra imaging and inForm software provided computer automated random high power field selection and counting of positively stained cells, allowing for an objective and uniform assessment of immunohistochemical staining. Traditionally, staining quantification by IHC is limited to a few high powered fields that are chosen based on areas of representative staining, and it is difficult to control for interpreter bias. In contrast, the true random selection of up to 30 HPFs in our study provides a more global reflection of the immune microenvironment of the samples, and is less likely to be biased by areas of sparse or concentrated staining. Furthermore, the identification of positive staining thresholds and computer quantification reduces inter- and intra-observer variability of positive cell counting.

It is also important to recognize the limitations of this new imaging and quantitation methodology. Despite improving the objectivity of IHC analysis in our study, some subjective measures are still used in the process of developing these methods, such as determination of positive signal thresholds and lack of 100% accuracy in identifying tumor and stroma compartments. Importantly, these limitations in the analysis would not be skewed towards any one group and would not change the trends in the immune markers seen. While multiplexing IHC panels empower analysis of multiple markers on a single tissue section, this methodology is particularly sensitive to batch effects and must be considered in both study design and analysis. Comparisons of markers between groups

must be confined to staining within a single batch (single panel), as demonstrated by the differences in PD-L1 and CD8 staining intensity among the panels. There are multiple reasons that may contribute to difference in staining intensity. Different temperatures used in antigen retrieval for the unique antibodies used in the different panels can impact antigen retrieval. Specifically, elevated temperatures used in multiplexing panel 1 may have enhanced antigen retrieval and staining intensity resulting in the increased intensity of PD-L1 staining in panel 1. Additionally, the IHC staining and processing of slides in this method is conducted manually. As such, there is likely to be some slight variation between timing across batches in any one of the 8 steps, in particular the 5 steps that are repeated up to 4 times. This points to the importance of ensuring that all slides are stained together and that comparisons can only be made within one batch. In this specific case, the consistent trend in stromal PD-L1 expression does support a difference in PD-L1 expression between MSI-H and MSS EC.

This study could be further improved by adding analysis of POLE mutation status as this EC molecular subtype has been shown to have an even more immunogenic microenvironment than MSI-H EC (56, 59). As these tumors tend to be MSS, the counts of immune cells and immune markers in the MSS group may have been elevated and resulted in a smaller overall difference in positive cell counts between the two groups. Despite this, stratifying patients by MSI status for consideration of immune checkpoint blockade is the most clinically feasible as patients with POLE mutations are much less likely to recur.

In considering next steps to further evaluate efficacy of immunotherapy in the MSI-H EC patient population, a phase 2 study evaluating response rates to immune checkpoint

blockade in patients with MSI-H and MSS EC is needed. A potential study design was created in collaboration Dr. Amir Jazaeri and is depicted in Figure 12. Briefly, such a study would include patients with advanced or recurrent EC that have failed initial standard chemotherapy. Patients with MSI-H tumors would make up the first arm and those with MSS tumors the second arm. Treatment would begin with a single agent anti-PD-1 or anti-PD-L1 therapy. Anti- CTLA-4 treatment would then be added for those that progressed or did not respond to single agent therapy, as combination anti-CTLA-4 and anti-PD-1 has previously shown improved responses to single agent therapy in other tumor types (65). This adaptive approach would help to maximize benefit from immune checkpoint blockade in the entire cohort by adding a second agent for non-responders, while also identifying those who do respond to a single agent to minimize adverse effects from an unnecessary second agent.

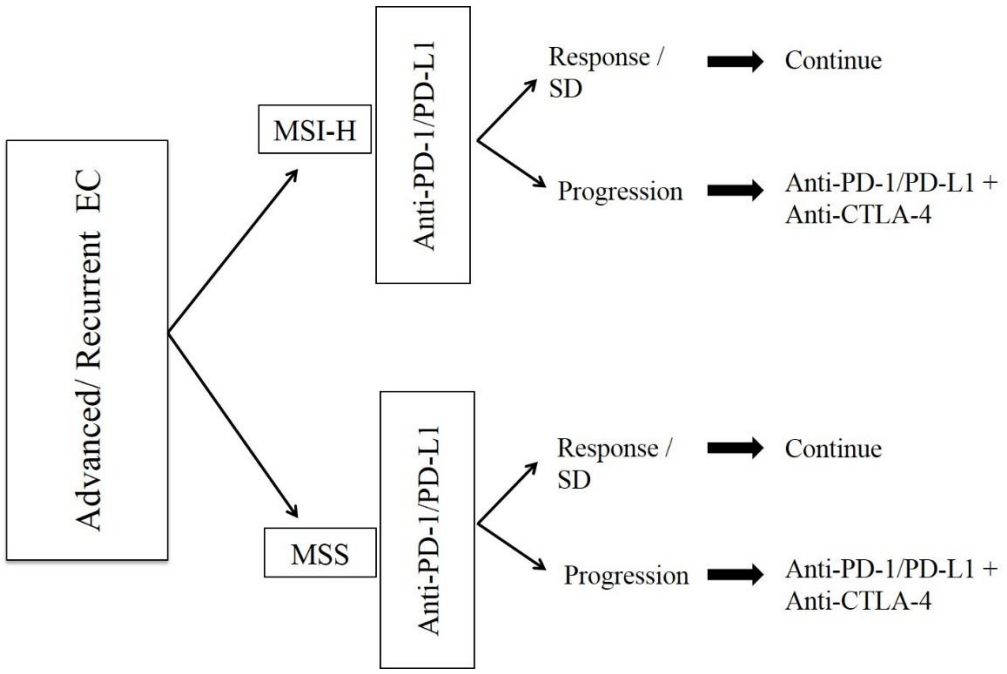

Figure 12. Proposed phase 2 trial to evaluate the role of immune checkpoint blockade in advanced and recurrent EC.

Abbreviations: EC, endometrial cancer; MSI-H, high microsatellite instability; MSS; microsatellite stable; SD, stable disease.

Chapter 5: Conclusions

In summary, this thesis shows that MSI-H ECs have an altered immune microenvironment compared to MSS ECs. Specifically, MSI-H EC compared to MSS EC demonstrated increased activation of the granzyme B pathway and elevated levels of activated CTLs. This increased cytolytic activity indicates an immune related anti-tumor response in MSI-H EC. Additionally, increased stromal PD-L1 expression was seen in all MSI-H EC versus MSS and suggests a shift to a pro-tumorigenic microenvironment and suppression of the immune response. As our understanding of the spectrum of patients benefiting from immunotherapy and immune checkpoint blockade widens, these therapies may prove to be advantageous in EC patients. Our finding of increased activated CTLs and stromal PD-L1 expression in MSI-H ECs identifies patients with this molecular subset of tumors as candidates for treatment with immunotherapy.

References

1. Siegel RL, Miller KD, Jemal A. 2016. Cancer statistics, 2016. *CA Cancer J Clin* 66: 7-30
2. Siegel RL MK, Jemal A. 2015. Cancer statistics, 2015. *CA: A Cancer Journal for Clinicians*
3. Creasman WT, Odicino F, Maisonneuve P, Quinn MA, Beller U, Benedet JL, Heintz AP, Ngan HY, Pecorelli S. 2006. Carcinoma of the corpus uteri. FIGO 26th Annual Report on the Results of Treatment in Gynecological Cancer. *Int J Gynaecol Obstet* 95 Suppl 1: S105-43
4. Backes FJ, Cohn DE. 2011. Lynch syndrome. *Clin Obstet Gynecol* 54: 199-214
5. Lu KH, Dinh M, Kohlmann W, Watson P, Green J, Syngal S, Bandipalliam P, Chen LM, Allen B, Conrad P, Terdiman J, Sun C, Daniels M, Burke T, Gershenson DM, Lynch H, Lynch P, Broaddus RR. 2005. Gynecologic cancer as a "sentinel cancer" for women with hereditary nonpolyposis colorectal cancer syndrome. *Obstet Gynecol* 105: 569-74
6. Wijnen J, de Leeuw W, Vasen H, van der Klift H, Moller P, Stormorken A, Meijers-Heijboer H, Lindhout D, Menko F, Vossen S, Moslein G, Tops C, Brocker-Vriends A, Wu Y, Hofstra R, Sijmons R, Cornelisse C, Morreau H, Fodde R. 1999. Familial endometrial cancer in female carriers of MSH6 germline mutations. *Nat Genet* 23: 142-4
7. Deligdisch L, Holinka CF. 1987. Endometrial carcinoma: two diseases? *Cancer Detect Prev* 10: 237-46
8. Cancer Genome Atlas Research N, Kandoth C, Schultz N, Cherniack AD, Akbani R, Liu Y, Shen H, Robertson AG, Pashtan I, Shen R, Benz CC, Yau C, Laird PW, Ding L, Zhang W, Mills GB, Kucherlapati R, Mardis ER, Levine DA. 2013. Integrated genomic characterization of endometrial carcinoma. *Nature* 497: 67-73
9. Liu Y, Patel L, Mills GB, Lu KH, Sood AK, Ding L, Kucherlapati R, Mardis ER, Levine DA, Shmulevich I, Broaddus RR, Zhang W. 2014. Clinical significance of CTNNB1 mutation and Wnt pathway activation in endometrioid endometrial carcinoma. *J Natl Cancer Inst* 106
10. Salvesen HB, MacDonald N, Ryan A, Iversen OE, Jacobs IJ, Akslen LA, Das S. 2000. Methylation of hMLH1 in a population-based series of endometrial carcinomas. *Clin Cancer Res* 6: 3607-13

11. Burks RT, Kessis TD, Cho KR, Hedrick L. 1994. Microsatellite instability in endometrial carcinoma. *Oncogene* 9: 1163-6

12. Helland A, Borresen-Dale AL, Peltomaki P, Hektoen M, Kristensen GB, Nesland JM, de la Chapelle A, Lothe RA. 1997. Microsatellite instability in cervical and endometrial carcinomas. *Int J Cancer* 70: 499-501

13. Goodfellow PJ, Billingsley CC, Lankes HA, Ali S, Cohn DE, Broaddus RJ, Ramirez N, Pritchard CC, Hampel H, Chassen AS, Simmons LV, Schmidt AP, Gao F, Brinton LA, Backes F, Landrum LM, Geller MA, DiSilvestro PA, Pearl ML, Lele SB, Powell MA, Zaino RJ, Mutch D. 2015. Combined Microsatellite Instability, MLH1 Methylation Analysis, and Immunohistochemistry for Lynch Syndrome Screening in Endometrial Cancers From GOG210: An NRG Oncology and Gynecologic Oncology Group Study. *J Clin Oncol* 33: 4301-8

14. Mills AM, Liou S, Ford JM, Berek JS, Pai RK, Longacre TA. 2014. Lynch syndrome screening should be considered for all patients with newly diagnosed endometrial cancer. *Am J Surg Pathol* 38: 1501-9

15. Gryfe R, Kim H, Hsieh ET, Aronson MD, Holowaty EJ, Bull SB, Redston M, Gallinger S. 2000. Tumor microsatellite instability and clinical outcome in young patients with colorectal cancer. *N Engl J Med* 342: 69-77

16. Zhu L, Li Z, Wang Y, Zhang C, Liu Y, Qu X. 2015. Microsatellite instability and survival in gastric cancer: A systematic review and meta-analysis. *Mol Clin Oncol* 3: 699-705

17. Ribic CM, Sargent DJ, Moore MJ, Thibodeau SN, French AJ, Goldberg RM, Hamilton SR, Laurent-Puig P, Gryfe R, Shepherd LE, Tu D, Redston M, Gallinger S. 2003. Tumor microsatellite-instability status as a predictor of benefit from fluorouracil-based adjuvant chemotherapy for colon cancer. *N Engl J Med* 349: 247-57

18. Carethers JM, Smith EJ, Behling CA, Nguyen L, Tajima A, Doctolero RT, Cabrera BL, Goel A, Arnold CA, Miyai K, Boland CR. 2004. Use of 5-fluorouracil and survival in patients with microsatellite-unstable colorectal cancer. *Gastroenterology* 126: 394-401

19. Diaz-Padilla I, Romero N, Amir E, Matias-Guiu X, Vilar E, Muggia F, Garcia-Donas J. 2013. Mismatch repair status and clinical outcome in endometrial cancer: a systematic review and meta-analysis. *Crit Rev Oncol Hematol* 88: 154-67

20. Meyer LA, Broaddus RR, Lu KH. 2009. Endometrial Cancer and Lynch Syndrome: Clinical and Pathologic Considerations. *Cancer control : journal of the Moffitt Cancer Center* 16: 14-22

21. Pijnenborg JM, Dam-de Veen GC, de Haan J, van Engeland M, Groothuis PG. 2004. Defective mismatch repair and the development of recurrent endometrial carcinoma. *Gynecol Oncol* 94: 550-9

22. Dellinger TH, Monk BJ. 2009. Systemic therapy for recurrent endometrial cancer: a review of North American trials. *Expert Rev Anticancer Ther* 9: 905-16

23. Dizon DS. 2010. Treatment options for advanced endometrial carcinoma. *Gynecol Oncol* 117: 373-81

24. Bradford LS, Rauh-Hain JA, Schorge J, Birrer MJ, Dizon DS. 2015. Advances in the management of recurrent endometrial cancer. *Am J Clin Oncol* 38: 206-12

25. Oza AM, Elit L, Tsao MS, Kamel-Reid S, Biagi J, Provencher DM, Gotlieb WH, Hoskins PJ, Ghatage P, Tonkin KS, Mackay HJ, Mazurka J, Sederias J, Ivy P, Dancey JE, Eisenhauer EA. 2011. Phase II study of temsirolimus in women with recurrent or metastatic endometrial cancer: a trial of the NCIC Clinical Trials Group. *J Clin Oncol* 29: 3278-85

26. Slomovitz BM, Lu KH, Johnston T, Coleman RL, Munsell M, Broaddus RR, Walker C, Ramondetta LM, Burke TW, Gershenson DM, Wolf J. 2010. A phase 2 study of the oral mammalian target of rapamycin inhibitor, everolimus, in patients with recurrent endometrial carcinoma. *Cancer* 116: 5415-9

27. Tsoref D, Welch S, Lau S, Biagi J, Tonkin K, Martin LA, Ellard S, Ghatage P, Elit L, Mackay HJ, Allo G, Tsao MS, Kamel-Reid S, Eisenhauer EA, Oza AM. 2014. Phase II study of oral ridaforolimus in women with recurrent or metastatic endometrial cancer. *Gynecol Oncol* 135: 184-9

28. Aghajanian C, Sill MW, Darcy KM, Greer B, McMeekin DS, Rose PG, Rotmensch J, Barnes MN, Hanjani P, Leslie KK. 2011. Phase II trial of bevacizumab in recurrent or persistent endometrial cancer: a Gynecologic Oncology Group study. *J Clin Oncol* 29: 2259-65

29. Oza AM, Eisenhauer EA, Elit L, Cutz JC, Sakurada A, Tsao MS, Hoskins PJ, Biagi J, Ghatage P, Mazurka J, Provencher D, Dore N, Dancey J, Fyles A. 2008. Phase II study of erlotinib in recurrent or metastatic endometrial cancer: NCIC IND-148. *J Clin Oncol* 26: 4319-25

30. Segal NH, Parsons DW, Peggs KS, Velculescu V, Kinzler KW, Vogelstein B, Allison JP. 2008. Epitope landscape in breast and colorectal cancer. *Cancer Res* 68: 889-92

31. Maher J, Davies ET. 2004. Targeting cytotoxic T lymphocytes for cancer immunotherapy. *Br J Cancer* 91: 817-21

32. Gooden MJ, de Bock GH, Leffers N, Daemen T, Nijman HW. 2011. The prognostic influence of tumour-infiltrating lymphocytes in cancer: a systematic review with meta-analysis. *Br J Cancer* 105: 93-103

33. Sato E, Olson SH, Ahn J, Bundy B, Nishikawa H, Qian F, Jungbluth AA, Frosina D, Gnjatic S, Ambrosone C, Kepner J, Odunsi T, Ritter G, Lele S, Chen YT, Ohtani H, Old LJ, Odunsi K. 2005. Intraepithelial CD8+ tumor-infiltrating lymphocytes and a high CD8+/regulatory T cell ratio are associated with favorable prognosis in ovarian cancer. *Proc Natl Acad Sci U S A* 102: 18538-43

34. Oble DA, Loewe R, Yu P, Mihm MC, Jr. 2009. Focus on TILs: prognostic significance of tumor infiltrating lymphocytes in human melanoma. *Cancer Immun* 9: 3

35. Eguizabal C, Zenarruzabeitia O, Monge J, Santos S, Vesga MA, Maruri N, Arrieta A, Rinon M, Tamayo-Orbegozo E, Amo L, Larrucea S, Borrego F. 2014. Natural killer cells for cancer immunotherapy: pluripotent stem cells-derived NK cells as an immunotherapeutic perspective. *Front Immunol* 5: 439

36. Kennedy R, Celis E. 2008. Multiple roles for CD4+ T cells in anti-tumor immune responses. *Immunol Rev* 222: 129-44

37. Lewis CE, Pollard JW. 2006. Distinct role of macrophages in different tumor microenvironments. *Cancer Res* 66: 605-12

38. Knutson KL, Disis ML. 2005. Tumor antigen-specific T helper cells in cancer immunity and immunotherapy. *Cancer Immunol Immunother* 54: 721-8

39. Topalian SL, Drake CG, Pardoll DM. 2015. Immune checkpoint blockade: a common denominator approach to cancer therapy. *Cancer Cell* 27: 450-61

40. Taube JM, Anders RA, Young GD, Xu H, Sharma R, McMiller TL, Chen S, Klein AP, Pardoll DM, Topalian SL, Chen L. 2012. Colocalization of inflammatory response with B7-h1 expression in human melanocytic lesions supports an adaptive resistance mechanism of immune escape. *Sci Transl Med* 4: 127ra37

41. Taube JM, Klein A, Brahmer JR, Xu H, Pan X, Kim JH, Chen L, Pardoll DM, Topalian SL, Anders RA. 2014. Association of PD-1, PD-1 ligands, and other features of the tumor immune microenvironment with response to anti-PD-1 therapy. *Clin Cancer Res* 20: 5064-74

42. Herbst RS, Soria JC, Kowanetz M, Fine GD, Hamid O, Gordon MS, Sosman JA, McDermott DF, Powderly JD, Gettinger SN, Kohrt HE, Horn L, Lawrence DP, Rost S, Leabman M, Xiao Y, Mokatrin A, Koeppen H, Hegde PS, Mellman I, Chen DS, Hodi FS. 2014. Predictive correlates of response to the anti-PD-L1 antibody MPDL3280A in cancer patients. *Nature* 515: 563-7

43. Postow MA, Chesney J, Pavlick AC, Robert C, Grossmann K, McDermott D, Linette GP, Meyer N, Giguere JK, Agarwala SS, Shaheen M, Ernstoff MS, Minor D, Salama AK, Taylor M, Ott PA, Rollin LM, Horak C, Gagnier P, Wolchok JD, Hodi FS. 2015. Nivolumab and ipilimumab versus ipilimumab in untreated melanoma. *N Engl J Med* 372: 2006-17

44. Topalian SL, Hodi FS, Brahmer JR, Gettinger SN, Smith DC, McDermott DF, Powderly JD, Carvajal RD, Sosman JA, Atkins MB, Leming PD, Spigel DR, Antonia SJ, Horn L, Drake CG, Pardoll DM, Chen L, Sharfman WH, Anders RA, Taube JM, McMiller TL, Xu H, Korman AJ, Jure-Kunkel M, Agrawal S, McDonald D, Kollia GD, Gupta A, Wigginton JM, Sznol M. 2012. Safety, Activity, and Immune Correlates of Anti–PD-1 Antibody in Cancer. *New England Journal of Medicine* 366: 2443-54

45. Brahmer JR, Tykodi SS, Chow LQM, Hwu W-J, Topalian SL, Hwu P, Drake CG, Camacho LH, Kauh J, Odunsi K, Pitot HC, Hamid O, Bhatia S, Martins R, Eaton K, Chen S, Salay TM, Alaparthy S, Grosso JF, Korman AJ, Parker SM, Agrawal S, Goldberg SM, Pardoll DM, Gupta A, Wigginton JM. 2012. Safety and Activity

of Anti–PD-L1 Antibody in Patients with Advanced Cancer. *New England Journal of Medicine* 366: 2455-65

46. Clarke B, Tinker AV, Lee CH, Subramanian S, van de Rijn M, Turbin D, Kalloger S, Han G, Ceballos K, Cadungog MG, Huntsman DG, Coukos G, Gilks CB. 2009. Intraepithelial T cells and prognosis in ovarian carcinoma: novel associations with stage, tumor type, and BRCA1 loss. *Mod Pathol* 22: 393-402

47. Gorfu G, Rivera-Nieves J, Ley K. 2009. Role of beta7 integrins in intestinal lymphocyte homing and retention. *Curr Mol Med* 9: 836-50

48. Webb JR, Milne K, Watson P, Deleeuw RJ, Nelson BH. 2014. Tumor-infiltrating lymphocytes expressing the tissue resident memory marker CD103 are associated with increased survival in high-grade serous ovarian cancer. *Clin Cancer Res* 20: 434-44

49. Ling KL, Dulphy N, Bahl P, Salio M, Maskell K, Piris J, Warren BF, George BD, Mortensen NJ, Cerundolo V. 2007. Modulation of CD103 expression on human colon carcinoma-specific CTL. *J Immunol* 178: 2908-15

50. Llosa NJ, Cruise M, Tam A, Wicks EC, Hechenbleikner EM, Taube JM, Blosser RL, Fan H, Wang H, Luber BS, Zhang M, Papadopoulos N, Kinzler KW, Vogelstein B, Sears CL, Anders RA, Pardoll DM, Housseau F. 2015. The Vigorous Immune Microenvironment of Microsatellite Instable Colon Cancer Is Balanced by Multiple Counter-Inhibitory Checkpoints. *Cancer Discovery* 5: 43-51

51. Phillips SM, Banerjea A, Feakins R, Li SR, Bustin SA, Dorudi S. 2004. Tumour-infiltrating lymphocytes in colorectal cancer with microsatellite instability are activated and cytotoxic. *British Journal of Surgery* 91: 469-75

52. Le DT, Uram JN, Wang H, Bartlett BR, Kemberling H, Eyring AD, Skora AD, Luber BS, Azad NS, Laheru D, Biedrzycki B, Donehower RC, Zaheer A, Fisher GA, Crocenzi TS, Lee JJ, Duffy SM, Goldberg RM, de la Chapelle A, Koshiji M, Bhaijee F, Huebner T, Hruban RH, Wood LD, Cuka N, Pardoll DM, Papadopoulos N, Kinzler KW, Zhou S, Cornish TC, Taube JM, Anders RA, Eshleman JR, Vogelstein B, Diaz LA, Jr. 2015. PD-1 Blockade in Tumors with Mismatch-Repair Deficiency. *N Engl J Med* 372: 2509-20

53. A.N. Fader LAD, D.K. Armstrong, E.J. Tanner III, J. Urama, A. Eyring, H. Wang, G. Fisher, T. Greten and D., Le. 2016. Preliminary results of a phase II study: PD-1 blockade in mismatch repair–deficient, recurrent or persistent endometrial cancer. 47th Annual Meeting of the Society of Gynecologic Oncology

54. Kondratiev S, Sabo E, Yakirevich E, Lavie O, Resnick MB. 2004. Intratumoral CD8+ T lymphocytes as a prognostic factor of survival in endometrial carcinoma. *Clin Cancer Res* 10: 4450-6

55. Dun EC, Hanley K, Wieser F, Bohman S, Yu J, Taylor RN. 2013. Infiltration of tumor-associated macrophages is increased in the epithelial and stromal compartments of endometrial carcinomas. *Int J Gynecol Pathol* 32: 576-84

56. Howitt BE, Shukla SA, Sholl LM, et al. 2015. ASsociation of polymerase e–mutated and microsatellite-instable endometrial cancers with neoantigen load,

number of tumor-infiltrating lymphocytes, and expression of pd-1 and pd-l1. *JAMA Oncology*

57. Risinger JI, Chandramouli GVR, Larry Maxwell G, Litzi T, Berchuck A, Umar A. 2006. Gene expression analysis of tumor infiltrating lymphocyte markers in endometrial cancers indicates no significant increases in those cases with microsatellite instability. *Cancer Biomarkers* 2: 61-8

58. Shia J, Black D, Hummer AJ, Boyd J, Soslow RA. 2008. Routinely assessed morphological features correlate with microsatellite instability status in endometrial cancer. *Human Pathology* 39: 116-25

59. van Gool IC, Eggink FA, Freeman-Mills L, Stelloo E, Marchi E, de Bruyn M, Palles C, Nout RA, de Kroon CD, Osse EM, Klenerman P, Creutzberg CL, Tomlinson IP, Smit VT, Nijman HW, Bosse T, Church DN. 2015. POLE Proofreading Mutations Elicit an Antitumor Immune Response in Endometrial Cancer. *Clin Cancer Res* 21: 3347-55

60. Rahman M, Jackson LK, Johnson WE, Li DY, Bild AH, Piccolo SR. 2015. Alternative preprocessing of RNA-Sequencing data in The Cancer Genome Atlas leads to improved analysis results. *Bioinformatics* 31: 3666-72

61. Lal N, Beggs AD, Willcox BE, Middleton GW. 2015. An immunogenomic stratification of colorectal cancer: Implications for development of targeted immunotherapy. *Oncoimmunology* 4: e976052

62. Vilar E, Mork ME, Cuddy A, Borras E, Bannon SA, Taggart MW, Ying J, Broaddus RR, Luthra R, Rodriguez-Bigas MA, Lynch PM, You YQ. 2014. Role of microsatellite instability-low as a diagnostic biomarker of Lynch syndrome in colorectal cancer. *Cancer Genet* 207: 495-502

63. Bruegl AS, Djordjevic B, Batte B, Daniels M, Fellman B, Urbauer D, Luthra R, Sun C, Lu KH, Broaddus RR. 2014. Evaluation of clinical criteria for the identification of Lynch syndrome among unselected patients with endometrial cancer. *Cancer Prev Res (Phila)* 7: 686-97

64. Stack EC, Wang C, Roman KA, Hoyt CC. 2014. Multiplexed immunohistochemistry, imaging, and quantitation: a review, with an assessment of Tyramide signal amplification, multispectral imaging and multiplex analysis. *Methods* 70: 46-58

65. Larkin J, Chiarion-Sileni V, Gonzalez R, Grob JJ, Cowey CL, Lao CD, Schadendorf D, Dummer R, Smylie M, Rutkowski P, Ferrucci PF, Hill A, Wagstaff J, Carlino MS, Haanen JB, Maio M, Marquez-Rodas I, McArthur GA, Ascierto PA, Long GV, Callahan MK, Postow MA, Grossmann K, Sznol M, Dreno B, Bastholt L, Yang A, Rollin LM, Horak C, Hodi FS, Wolchok JD. 2015. Combined Nivolumab and Ipilimumab or Monotherapy in Untreated Melanoma. *N Engl J Med* 373: 23-34

66. Le DT, Uram JN, Wang H, Bartlett BR, Kemberling H, Eyring AD, Skora AD, Luber BS, Azad NS, Laheru D, Biedrzycki B, Donehower RC, Zaheer A, Fisher GA, Crocenzi TS, Lee JJ, Duffy SM, Goldberg RM, de la Chapelle A, Koshiji M,

Bhaijee F, Huebner T, Hruban RH, Wood LD, Cuka N, Pardoll DM, Papadopoulos N, Kinzler KW, Zhou S, Cornish TC, Taube JM, Anders RA, Eshleman JR, Vogelstein B, Diaz LA. 2015. PD-1 Blockade in Tumors with Mismatch-Repair Deficiency. *New England Journal of Medicine* 372: 2509-20

67. Le Floc'h A, Jalil A, Franciszkiewicz K, Validire P, Vergnon I, Mami-Chouaib F. 2011. Minimal engagement of CD103 on cytotoxic T lymphocytes with an E-cadherin-Fc molecule triggers lytic granule polarization via a phospholipase Cgamma-dependent pathway. *Cancer Res* 71: 328-38

68. Antonia SJ GS, Chow LQM, Juergens RA, Borghaei H, Shen Y, Harbison C, Chen AC, Ready N, Rizvi NA. 2014. Nivolumab (anti-PD-1; BMS-936558, ONO-4538) and ipilumumab in first-line NSCLC: Interim phase I results. . *ASCO Meeting Abstracts* 32(15_suppl)

69. Woo SR, Turnis ME, Goldberg MV, Bankoti J, Selby M, Nirschl CJ, Bettini ML, Gravano DM, Vogel P, Liu CL, Tangsombatvisit S, Grosso JF, Netto G, Smeltzer MP, Chaux A, Utz PJ, Workman CJ, Pardoll DM, Korman AJ, Drake CG, Vignali DA. 2012. Immune inhibitory molecules LAG-3 and PD-1 synergistically regulate T-cell function to promote tumoral immune escape. *Cancer Res* 72: 917-27

70. Liu J, Zhang S, Hu Y, Yang Z, Li J, Liu X, Deng L, Wang Y, Zhang X, Jiang T, Lu X. 2016. Targeting PD-1 and Tim-3 Pathways to Reverse CD8 T-Cell Exhaustion and Enhance Ex Vivo T-Cell Responses to Autologous Dendritic/Tumor Vaccines. *J Immunother* 39: 171-80

71. Papadimitrakopoulou V PA, Borghaei H, Stevenson J, Gandhi L, Gubens MA, Yang JCH, Sequist LV, Ge JY, Bourque J, Bachman RD, Im E, Gadgeel SM. 2015. Pembrolizumab (pembro; MK-3475) plus paltinum doublet chemotherapy (PDC) as front-line therapy for advanced non-small cell lung cancer (NSCLC): KEYNOTE-021 Cohorts A and C. *J Clin Oncol* 33(suppl; abstr 8031)

72. Liu SV PJ, Camidge DR, Ready N, Heist RS, Hodi S, Giaccone G, Liu B, Wallin J, Funke RP, Gettinger SN. 2105. Safety and efficacy of MPDL3280A (anti-PDL1) in combination with platinum-based doublet chemotherapy in patients with advanced non-small cell lung cancer (NSCLC). *J Clin Oncol* 33(suppl;abstr 8030)

Vita

Janelle Pakish, M.D. was born in Nampa, Idaho on October 6, 1983 to John and Donna Pakish. She attended the University of Pennsylvania and received a Bachelor of Arts degree in biology with a concentration in molecular biology in 2006. She then received her Doctor of Medicine from the University of Washington School of Medicine in 2010. She went on to complete an obstetrics and gynecology residency at Dartmouth-Hitchcock Medical Center in 2014 where she had experience teaching both medical students and junior residents. She is currently a gynecologic oncology fellow at the University of Texas, M.D. Anderson Cancer Center and will complete her training in June 2018. Her publications have included retrospective reviews of adjuvant treatment in non-small cell lung cancer and approaches to para-aortic lymphadenectomy in endometrial cancer staging.

Permanent address:
1 Hermann Park Ct., Apt. 842
Houston, TX 77021